10-5-2017

EXPERIMENTAL STUDY ON REHABILITATION OF CORRODED PIPES

Sachith Jayasuriya
University of Windsor

EXPERIMENTAL STUDY ON REHABILITATION OF CORRODED PIPES

By

Sachith Jayasuriya

A Thesis
Submitted to the Faculty of Graduate Studies
through the Department of Civil and Environmental Engineering
in Partial Fulfillment of the Requirements for
the Degree of Master of Applied Science
at the University of Windsor

Windsor, Ontario, Canada

2017

EXPERIMENTAL STUDY ON REHABILITATION OF CORRODED PIPES

By

Sachith Jayasuriya

APPROVED BY:

S. Chowdhury
Department of Electrical and Computer Engineering

S. Cheng
Department of Civil and Environmental Engineering

S. Das, Advisor
Department of Civil and Environmental Engineering

T. Bolisetti, Co-advisor
Department of Civil and Environmental Engineering

September 19, 2017

DECLARATION OF CO-AUTHORSHIP

I hereby declare that this thesis incorporates material that is result of joint research, as follows:

This thesis is a product of the joint research conducted in collaboration with Behrouz Chengi under the supervision of Dr. S. Das and Dr. T. Bolisetti. In all cases, the key ideas, primary contributions, experimental designs, data analysis, interpretation, and writing were performed by the author, and the contribution of co-author, Behrouz Chengi, was primarily through the advice and assistance in experimental testing.

I am aware of the University of Windsor Senate Policy on Authorship and I certify that I have properly acknowledged the contribution of other researchers to my thesis, and have obtained written permission from each of the co-author(s) to include the above material(s) in my thesis.

I certify that, with the above qualification, this thesis, and the research to which it refers, is the product of my own work.

I declare that, to the best of my knowledge, my thesis does not infringe upon anyone's copyright nor violate any proprietary rights and that any ideas, techniques, quotations, or any other material from the work of other people included in my thesis, published or otherwise, are fully acknowledged in accordance with the standard referencing practices. Furthermore, to the extent that I have included copyrighted material that surpasses the bounds of fair dealing within the meaning of the Canada Copyright Act, I certify that I have obtained a written permission from the copyright owner(s) to include such material(s) in my thesis.

I declare that this is a true copy of my thesis, including any final revisions, as approved by my thesis committee and the Graduate Studies office, and that this thesis has not been submitted for a higher degree to any other University or Institution.

ABSTRACT

Corrosion is a severe problem that affects oil and gas pipelines all over the world. When combined with the complex loading combinations faced by buried pipelines, the effects of corrosion can be devastating. Corrosion decreases the burst pressure, longitudinal load-capacity, and lateral load-capacity of affected pipes. Much research has been conducted to address this problem, and many repair techniques have been developed, including the use of fibre-reinforced polymers (FRPs). Most of the research that has been conducted on the use of FRP composites to repair pipes is concerned with increasing the burst pressure. The purpose of this study is to use a relatively new fibre, basalt, to increase the bending capacity of corroded pipes. To this end, five full-scale lab experiments and finite element analysis was conducted. It was found that a composite made of basalt fabric can increase the ultimate load of a pipe in bending. However, only a pipe specimen with a corrosion depth of 20% of the wall thickness could fully recover the bending capacity to that of an uncorroded pipe through the use of basalt FRP (BFRP) composite. Analysis of different thicknesses of BFRP composites and different orientations of the fabric using finite element analysis software indicated that increasing the amount of BFRP layers only yields a marginal increase in strength when bending.

ACKNOWLEDGEMENTS

I wish to express my sincere gratitude to Dr. Das and Dr. Bolisetti for providing me an opportunity to do my master's research under their supervision, as well as their guidance and encouragement throughout this project. I would also like to thank the committee members: Dr. Cheng and Dr. Chowdhury, for their thoughtful suggestions to improve this thesis.

I am also grateful towards Matt St. Louis, Lucian Pop, Andy Jenner, my brother and my friends Amirreza Bastani, Emad Booya, Behrouz Chegeni, Jothiarun Dhanapal, Hossein Ghaednia, Eric Hughes, Navjot Singh and Jamshid Zohreh Heydariha who helped me greatly in the lab. Without everyone's assistance, this project would not have been completed.

Finally, I would like to thank my family for the support and encouragement that they have given me during this project.

TABLE OF CONTENTS

Chapter 3: Experimental Program

Chapter 4: Experimental Results

Chapter 5: Finite Element Analysis

LIST OF TABLES

Chapter 3

Chapter 4

Chapter 5

LIST OF FIGURES

Chapter 1

Chapter 2

Chapter 3

Chapter 4

Chapter 5

LIST OF SYMBOLS

A	Effective area of missing metal
A_0	Original area
A_1	A factor used to determine P' (ASME B31G)
B	A constant which depends on the corrosion depth (ASME B31G)
d	Depth of corrosion
D	Outer diameter of the pipe
D/t	Diameter-to-thickness ratio of the pipe
D_0	Outer Diameter of the pipe
E	Young's modulus
E_a	Tensile modulus of the composite laminate in the axial direction
E_{ac}	$\sqrt{E_a \cdot E_c}$ (ASME PCC-2)
E_c	Tensile modulus for the composite laminate in the circumferential direction
E_s	Tensile modulus for substrate material
f	Service factor (ASME PCC-2)
F	Design factor (CSA Z662)
F	Design factor from ASMEB 31.4, ASME B31.8, ASME B31.11
F_a	Sum of axial tensile loads due to pressure, bending, and axial thrust
F_{ax}	Applied axial load
F_{eq}	Equivalent axial load
F_{sh}	Applied shear load
f_T	Temperature derating factor (ASME PCC-2)
L	Location Factor (CSA Z662)
L	Maximum allowable longitudinal length of corroded area (ASME B31G)

L_{defect}	Axial length of defect
L_{over}	Overlap length of repair
L_{repair}	Axial length of repair
L_{taper}	Length of taper
M	Stress magnification factor
M_{ax}	Applied axial load
M_{max}	Buckling moment of the pipe
M_{to}	Applied torsional moment
n	The number of measurements taken for the Effective Area Method
P	Internal design pressure
P'	Maximum pressure that is determined to be safe for the corroded section
P_b	Burst pressure of the pipe
P_{live}	Internal pressure within the pipe during the repair application
P_s	Maximum allowable operating pressure
p_y	Yield pressure
r	Outer radius of the pipe
S	Allowable stress of the substrate material
s	SMYS
S_F	The estimated failure stress of the pipe
S_{flow}	Flow stress
T	Temperature factor (CSA Z662)
t	Wall thickness of the pipe
T_h	Tensile strength of the composite in the hoop direction (CSA Z662)
t_{min}	Minimum repair thickness
t_{repair}	Design repair thickness

t_s	Minimum remaining wall thickness of the pipe
w	Design thickness of the fibre-reinforced composite (CSA Z662)
W	Width of slot defect
z	A factor used to calculate the stress magnification factor (ASME B31G)
γ	Toughness parameter of the composite (ASME PCC-2)
ε_a	Allowable axial strain of the laminate
ε_c	Allowable circumferential strain of the laminate
v_{ca}	Poisson's ratio of the composite laminate in the circumferential direction
υ	${v_{ca}}^2 \cdot E_a/E_c$ (ASME PCC-2)

LIST OF ABBREVIATIONS

BFRP	Basalt Fibre Reinforced Polymer
CFRP	Carbon Fibre Reinforced Polymer
FRP	Fibre Reinforced Polymer
GFRP	Glass Fibre Reinforced Polymer
LVDT	Linear Variable Differential Transformer
MAOP	Maximum Allowable Operating Pressure
NPS	Nominal Pipe Size
SMTS	Specified Minimum Tensile Strength
SMYS	Specified Minimum Yield Strength

Chapter 1 Introduction

1.1 General

A major problem facing the oil and gas industry is the corrosion of the pipelines that are used to transport the products. Corrosion is the slow break down of a material through chemical reactions. Corrosion affects not only pipelines, but other infrastructure such as bridges, sewers, and water treatment facilities. A study was released in 2002 by CC Technologies Laboratories, Inc. with support from the FHWA (Federal Highway Administration) and NACE International which provides a very comprehensive look at the impact of corrosion on America's economy. The objective of the study was to determine the impacts of corrosion on the economy and find cost-effective strategies to manage corrosion.

The study states that the estimated annual cost of metallic corrosion in the U.S. is $137.9 billion, which when extrapolated to the total U.S. economy totals to $276 billion, 3.1% of the U.S. Gross Domestic Product as of 1998(NACE International, 2002). One of the biggest contributors to this substantial cost is water and wastewater distribution systems ($36 billion) that need to be replaced or are in need of corrosion inhibitors. The World Corrosion Organization estimates that globally US$2.2 trillion is used to combat corrosion (Hays, n.d.). The repair of corroded pipelines as well as the catastrophic damage caused by the pipe failures cost billions of dollars each year to the economy. According to the report by CC Technologies, the cost of corrosion in the gas and liquid pipeline sector amounts to $7 billion annually in the U.S. (Figure 1.1)

Traditionally corrosion defects would be repaired with a steel sleeve enveloping the corroded area or by cutting and replacing the corroded section entirely. While these techniques are effective, they take a lot of time to complete, can be very costly and the use of hot-work near the volatile substances inside the pipe can be very dangerous.

1.2 Fibre Reinforced Polymers

In recent years many pipeline operators have opted to use FRP (Fibre Reinforced Polymer) repair techniques to restore the original strength of corroded pipes. Repairing pipelines using FRP materials is more attractive than using steel because of the ease of installation and often times can be done at a fraction of the cost of steel repair.

According to an article published in the November 2002 issue of Pipeline & Gas Journal by Jim Cuthill, carbon composite repairs can be used to withstand through-wall defects at the time of the repair or any time in the future, during the design life of the repair(Cuthill, 2002). He also went on to say that in some circumstances, the original substrate of entire pipe sections can be allowed to be subjected to complete corrosion without the loss of pipeline strength or pressure integrity. FRP composites have been used in many small-scale and large scale applications around the world. As stated by Jim Cuthill on the Pipeline & Gas Journal, more than three metric tons of carbon fibre and three metric tons of resin were used to make a 75-m long repair on a 60-inch steel saltwater feed line with extensive corrosion. The project, completed by FD Alliance (a partnership formed between DML Composites and Furmanite International), was completed at approximately 35-40% of the cost of replacement. CFRP composites have been used in the repair of gas lines operating at exceptionally high pressures and temperatures, such as a carbon steel gas compression line on the Amerada Hess Ltd floating production facility that was

deteriorating from external corrosion. The repair was completed by FD Alliance while the plant was live, and the pipeline was operating at 124^{o}C and 1160 psig.

A partner of the Natural Gas STAR program (a program intended to help reduce methane emissions) has reported saving over 106 million cubic feet of natural gas by choosing composite wrap as an alternative to pipeline replacement between 1993 and 1999. Use of composite wrap on gas pipelines as an alternative to older methods of repair can reduce safety risks, decrease pipeline downtime as pipeline repair is possible with shutting down gas flow, save gas for sale since purging of the pipeline is not required, and decrease methane emissions to the atmosphere because cutting into the pipe is not required. In some circumstances when the use of composites may not be the most economical option, which may be the case for long defects, some still prefer composite wrap over pipeline replacement. In such cases, factors such as urgency and speed of repair or lack of a back-up gas supply may outweigh the cost of repair and influence the project manager to select composite wrap systems due to their faster repairs. Composite wrap repair eliminates the need for special equipment or skilled labourers such as welders. In a case reported by a Natural Gas STAR partner, a 20-inch defect on a pipe was repaired using composite wrap sleeves in four hours by two trained workers, with the entire process – from excavation to reburial - taking only two days. Since the pipe was near a creek bed, it was beneficial to not cut the pipeline as that would expose the water in the creek to the material being transported in the pipe.

FRP composites are made of reinforcing fibre that is impregnated with resin. In a composite the fibres provide the strength and stiffness while the resin holds the fibres in place and transfer stresses between fibres. Good reinforcing fibres usually have a high

elastic modulus, high ultimate strength and sufficient elongation at fracture. The three most common types of fibres are carbon, glass and aramid.

1.3 Fibres

Carbon fibres have a lengthy manufacturing process which includes oxidation, carbonization and graphitization. Graphitization helps increase the elastic modulus of the fibres since graphite has a higher tensile modulus than carbon. The end result has high tensile strength and stiffness while being highly resistant to aggressive environments. However, carbon fibres have a very low elongation at failure with ultimate tensile strain varying between 0.5 and 1.1% (Burgoyne et al., 2007). The biggest drawback of carbon fibres is the cost, which is a result of the high price of the raw materials and the long process of carbonization and graphitization.

Glass fibre is made of silica, soda ash, lime and several other materials that is melted and drawn into continuous threads. Different additives are used during the fabrication process to improve the fibre's ability to become saturated by resin, improve the fibre's flexibility, and improve the strength of the bond. E-glass, the most common type of glass fibre, is used in a wide range of applications. However, in terms of tensile strength, ultimate tensile strain and Young's modulus it is inferior to the more expensive S-glass (Figure 1.2).

The term "aramid" is a combination of the words aromatic polyamide, which are fibres with the molecule chains aligned along the axis of the fibre. Due to the strength of this chemical bond aramid fibres are able to demonstrate high strength and stiffness. There are a few different types of aramid products available in the market including Kevlar,

Technora, SVM, and Twaron, among others. Twaron fibres are manufactured by spinning a liquid crystalline solution of PPTA polymer (p-phenylene terephthalamides) in concentrated sulfuric acid and extruding the solution through spinning holes. The specific method of production varies for each product. Consequently, the mechanical properties of aramid products vary between carbon fibres and glass fibres.

A relatively new fibre being studied for use in structural reinforcement is basalt. Even though the idea to extract fibres from basalt was first introduced in 1923 by Paul Dhè, compared to carbon and glass, not much research has been done on reinforcement abilities of basalt composites. Lately basalt fibres have been gaining a lot of interest due to its eco-friendly composition and relatively low cost.

Basalt Fibre Reinforced Polymers (BFRPs) are cost effective because the raw material used to make BFRP is basalt rock, the most abundant igneous rock on Earth. There are major basalt quarries concentrated in Russia, Georgia, Ukraine, China and eastern areas of the U.S.A making the raw material is easy to obtain. However, unlike glass which transmits infrared energy, basalt absorbs infrared energy forcing the manufacturers to hold the basalt rocks in the reservoir for an extended period of time in order for the melting basalt to be heated uniformly. As a result the cost of basalt fibres is higher than E-glass, but lower than S-glass and much lower than carbon fibres while the mechanical properties are comparable to S-glass. As the manufacturing of basalt fibres increases, the price of BFRP is expected to decrease.

The environmentally-friendly nature of basalt is due to the fact that the fibres are made entirely of basalt; no chemical additives, solvents or hazardous materials are included in

the melting process. As a result, no industrial waste is released during production and since basalt is inert, there is no toxic reaction with water or air.

1.4 Resins

Thermoset resins, as the name indicates are set when exposed to heat. Prior to curing the resin would be in a liquid state, then heat would be introduced, usually through a chemical reaction. Once cured the resin and the fibres that form the composite laminate become very rigid. This process cannot be reversed and the shape of the composite cannot be changed without chemically breaking down the resin-matrix. Some common types of resins include polyester, vinylester, polyutherene, silicone and epoxy. While epoxy tends to be the most costly resin, it offers relatively high mechanical properties.

Unlike thermoset resins, thermoplastic resins are solid in their natural state. When heated thermoplastic resins become soft or fluid. Since thermoplastic resins behave as a solid in its natural state, it is considerably harder to use them to impregnate the reinforcing fibres. The resin must first be melted so that it is fluid, then pressure is used to saturate the reinforcing fibres with the resin. When cooled down to room temperature under the same pressure, the composite becomes solid. While the process of manufacturing reinforcing composites using thermoplastic resins is harder, they offer a major advantage in their ability to change shape. When thermoplastic composites are heated their shape can be bent to have a curvature.

1.5 Objective

The objective of this research is to examine the effectiveness of basalt FRP (BFRP) composites in repairing corroded pipes subjected to bending. Large displacements due to

earthquakes, landslides, soil upheaval or snaking lead to the bending of pipelines. As the pipeline bends small ripples that are formed on the pipe localize into one or more large wrinkle depending on the curvature of the bend. If there is corrosion in a pipeline situated in areas with a lot of soil movement, or frost upheaval, the process would be accelerated. In order to alleviate the axial stress due to internal pressure or temperature fluctuations, the pipe will deform laterally in the corroded area (snaking) leading to wrinkling.

This research will be used to determine whether an FRP composite made of basalt fibre is able to restore the load carrying capacity of a corroded pipe to its original state and also whether it can change the buckling mode and stop the wrinkling process of a corroded pipe subjected to bending.

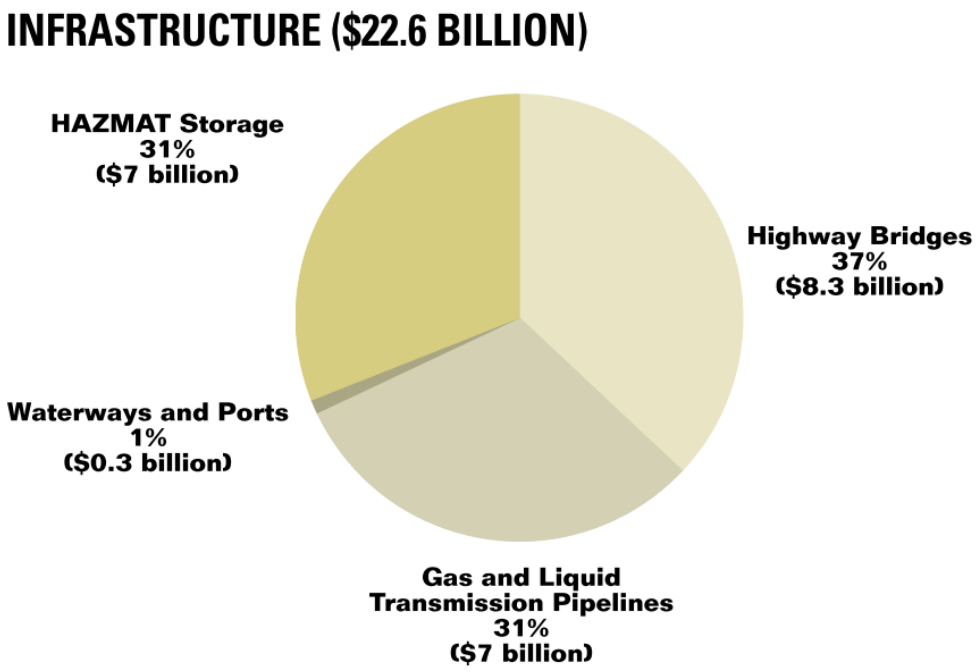

Figure 1.1: Annual cost of infrastructure in the U.S in 2002 (NACE International, 2002)

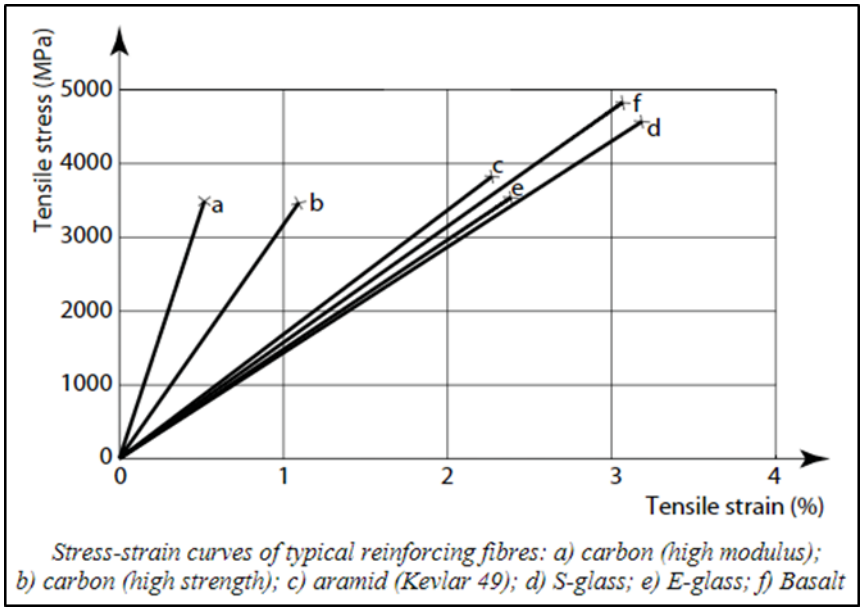

Figure 1.2: Mechanical properties of fibres (Burgoyne et. al, 2007)

Chapter 2 Literature Review

This literature review aims to summarize the information the author has found in the literature regarding bending of pipes, effects of corrosion, traditional repair techniques of pipes and the emerging composite repair techniques, as well as the current codes and standards that provide guidelines on pipeline repair.

2.1 Pipes Subjected to Bending

There have been a various studies conducted on the local buckling behaviour of tubes subjected to bending.

Ju and Kyriakides (1991) used unpressurized tubes of varying diameter-to-wall thickness (D/t) ratios to study the behaviour of cylindrical shells under bending. The study found that the tube cross-section initially shows uniform ovalization under bending. Then the tube buckles on the side subjected to compression and forms ripples. The study concluded that the limit load for buckling occurs at a curvature that is significantly lower than would be expected. The moment drops steeply after reaching the limit load. As the bending increases, the shell buckles further, as the ripple with the most severe deformation develops a sharp diamond-shaped kink.

Limam et. al (2010) studied the behaviour of pressurized tubes under bending. Similar to Ju and Kyriakides (1991), this study also found that the tube cross-section initially shows ovalization when bending. However, internal pressure helps reduce ovalization and causes the pipe to expand. The tube buckles on the compressive side under bending and forms wrinkles (Figure 2.1). As the bending increases, the amplitude of the wrinkles slowly increases until one wrinkle grows more prominently as an outward bulge and the

deformation and buckling localizes around this wrinkle. The work done by Ju and Kyriakides (1991) and Liamam et. al (2010) show that the presence of internal pressure is the cause of wrinkle formation in pipes subjected to bending since unpressurised pipes will fail with the development of an inwards kink (Figure 2.2).

Liamam et. al (2010) observed that the internal pressure can considerably delay localization and collapse of a pipe subjected to bending, noting that a pipe pressurized to 75% of yield pressure was able to withstand a collapse curvature at the point of collapse that is six times as much as the same pipe that was unpressurized. However, in order to realize this benefit of internal pressure, the pipe must be sufficiently ductile in order to avoid failure of the material before developing the bulge.

The findings by Limam et. al (2010) confirm the conclusions published by Yoosef-Ghodsi et. al (2000) that a buried pipeline that is deformed in axial compression or bending beyond its maximum capacity will form a wrinkle shaped defect. Yoosef-Ghodsi also stated that a pipe with a wrinkle defect can deform well into the post-wrinkling phase without rupturing.

Yudo and Yoshikawa (2015) analyzed the buckling strength of straight and curved pipes with varying lengths, diameters, thicknesses, and radius of curvatures of pipes using FE software. It was found that the buckling strength of the pipe is reduced due to the cross-sectional ovalization that occurs during the bending of the pipe. Since the ovalization is highest at the center, the buckling is limited to the compressive side of the midspan. According to the numerical calculations, buckling moment is reduced as oval

deformation of the pipe grows larger. Yudo and Yoshikawa proposed an equation to calculate the buckling moment for long pipes as

$$M_{max} = 0.314\pi Ert^2 \quad (2.1)$$

However, it is important to note that this equation does not take internal pressure into account.

2.2 Corrosion in pipes

Pipeline corrosion occurs due to a pipeline's interaction with its surroundings. In an article published by Prabhu (2016), the author states that most pipeline corrosion occurs due to an electrochemical reaction, where electrons from the surface of the pipe are transferred to nearby oxygen atoms, acids or cations of different metals. An electrolyte such as water must be present for the transfer of electrons to occur. As stated by Prabhu, there are internal and external factors affecting the corrosion rate of a pipeline. External factors consist of the surrounding environment of the pipe, such as the soil chemistry and moisture for buried pipelines and water chemistry for submerged pipelines. Internal factors affecting the corrosion rate include the properties of the gasses and liquids being carried, such as the oxygen content and reactivity levels, as well as the operating parameters of the pipeline: the temperature, flow rate and pressure. The interaction of dissimilar metals within the piping system can also lead to galvanic corrosion.

Prabhu outlined the following different types of common pipeline corrosion:

- Uniform Pipe Corrosion: thinning of the pipe caused by uniform loss of material along the surface of the pipe

- Pitting Corrosion: small cavities on a pipe surface caused localized deterioration due to material defects or an aggressive chemical.
- Selective Leaching (dealloying): corrosion of a solid alloy due to loss of an element that forms the alloy, through reactions with chemical substances that are in contact with the surface.
- Galvanic Corrosion: deterioration caused by coupling of dissimilar metals with an electrolyte (water, salt water). The metal more susceptible to corrosion becomes the anode and corrodes faster than it would by itself, while the other, metal becomes the cathode and corrodes slower than it would by itself. (Cathode is the negatively charged electrode, attracts positive charge (cations) and is the electron donor. Anode is the positively charged electrode, and it attracts electrons, is the source of positive charge in the coupling.)
- Crevice Corrosion: occurs in tight joints and crevices where the fluids may have become stagnant. The concentration of oxygen becomes lower than the surrounding water due to the crevice geometry which makes access into the crevice difficult. The corrosion now becomes an electrochemical reaction where the surface of the crevice is the anode. The anodic surface provides electrons to satisfy the reaction which in turn produces metal ions that hydrolyze and give off protons and forming corrosion products. The release of protons gives the crevice a strong positive charge that attracts negative ions in the environment, such as chlorides and sulfates. This leads the crevice to become more and more acidic, with pH levels sometimes equivalent to pure acids.
- Stray current Corrosion: is a chemical reaction driven by electricity from stray currents that were not intended to pass through the pipe. The chemical and electrical

reactions that occur in this process is similar to galvanic corrosion which produces current internally. However, since the external stray current is much higher than that possible by galvanic cells, the corrosion damage will be much higher as it is proportional to the strength of the passing stray current. Stray current corrosion occurs at the location where the current leaves the pipe. Once a stray current enters the pipeline, it may travel for some distance, seeking the path of least resistance. When the current leaves the pipeline, the location where the current leaves the pipeline will be left with localized pits and cavities.

2.3 Effects of Corrosion

When a pipe is subjected to corrosion, the load-carrying capacity of the pipe decreases as the corrosion slowly reduces the thickness of the pipe. Due to changes in temperature, either in the pipe's surroundings or the fluid that is carried inside the pipe, the pipe will expand or contract, creating axial stresses in the pipe walls. Also, ground movement, gradual or abrupt, can also create similar axial stresses. However, movements of the soil such as those caused by landslides, are more likely to act as transverse loads and subject the pipe to longitudinal bending. Many studies have been conducted to study the effect of corrosion on a pipe's axial and transverse load carrying capacity (Dewanbabee et. al, 2013) (Cosham and Hopkins, 2005).

The effect of corrosion on the performance of pipelines was studied by Dewanbabee et. al (2013) using ten full-scale lab tests and an FEA parametric study. The research was undertaken to study how corrosion affects the strength of pipes subjected to axial compression and internal pressure. This study consisted of eight lab tests with varying corrosion depths (25% and 50% of the pipe thickness), varying corrosion shape (square,

rectangular), and varying pressure ($0.2p_y$, $0.4p_y$) and two tests on control specimen with varying pressure ($0.2p_y$, $0.4p_y$). The study observed that increased corrosion depth reduces the net axial load capacity. It was found that not only the depth, but the shape of the corrosion also affects the performance of the pipe; Dewanbabee et. al (2010) concluded that increasing the corrosion in the direction of the circumference of the pipe reduces the net axial load capacity.

Elchalakani (2016) conducted 3-point bending test on circular hollow sections with varying corrosion depths and varying lengths of corrosion. The study found that increasing corrosion length along the longitudinal direction, significantly decreases the ultimate lateral load capacity.

Cosham and Hopkins (2005) developed a set of guide lines for assessing corrosion defects in pipelines, that can be used to assess pipeline defects. As summarized by Cosham and Hopkins, the longitudinal length of corrosion is much more important in controlling the burst strength of a pipe than the circumferential length under internal pressure loading. However, when axial or bending loads are introduced, the circumferential length must also be considered to determine the burst pressure. The study also found that defects that are short in length, typically less than three times the thickness of the pipe, does not reduce the burst pressure below the yield pressure of the uncorroded pipe.

The methods that can be used to prevent or control corrosion depend on various factors which include, among others, the specific material to be protected, what it comes into contact with, soil resistivity, humidity, and the type of environment in which it is located

(saltwater, industrial). Common methods of controlling corrosion involve protective coatings, corrosion resistant alloys, substituting metals with fibres and polymers, corrosion inhibitors, and cathodic protection (Prabhu, 2016).

Cathodic protection is a process in which a sacrificial anode is connected to the surface to be protected, creating an electrochemical cell where the surface being protected is the cathode. When in the presence of galvanic corrosion the sacrificial anode will corrode instead of the metal surface to which it is connected. This protection typically lasts 15-25 years (Peterborough Utilities Group).

The reduced load-carrying capacity of the pipelines due to corrosion can be very dangerous. Reduced wall thickness in sections of the pipeline can lead the pipe to burst from the internal pressure. Also, excessive deformation of those regions could cause a rupture in the pipe, leading to oil spills or natural gas leaks.

Natural gas, when leaked, is a contributor to global warming as it is made up of mostly methane. While natural gas does not present an immediate health and safety threat, the respiratory conditions of those exposed to gas leaks may be aggravated. On the other hand, an oil spill has much more dire effects on the environment, and the health and safety of nearby animals and humans. A leak in an oil pipeline causes pollution in the nearby area including land damage, water poisoning, and destruction of habitats. Exposure to the leaked oil could be fatal for animals; if the leak occurs underwater, fish and birds that prey on the fish will be highly susceptible. A leak in a pipeline will be very damaging to the owners of the pipeline as well, due to the loss of oil or gas, cost of the cleanup, and the risk of receiving negative public opinion. As a result, pipeline owners

take great care to repair or replace a pipeline before a leak can occur. Over the years many repair techniques have been developed to repair damaged sections of a pipe.

2.4 Traditional Repair Techniques

AEA Technology Consulting (2001) has prepared a report with guidelines for temporary and permanent pipe repair for England's Health and Safety Executive. The document covers a range of repair options applicable for the repair of most common types of pipe deterioration. The guide focuses mainly on metallic repair options such as clamps; however, a review of the use of composite materials for pipe repair has also been included.

The most basic method of pipeline repair consists of welding a curved, metallic patch over a small defect. This repair option is not suitable for high integrity applications. The patch clamp, a similar technique, uses a metallic clamp that is bolted closed longitudinally, with an elastomeric seal used to secure the damaged area. If the external surface of the pipe is damaged to an extent where the elastomeric seal cannot achieve proper contact, filler material may need to be used to restore the original geometry of the pipe surface. A similar device, the pin-hole repair clamp is a specialized tool that can be used to repair pin hole leaks found in pipes.

For higher-integrity applications, medium- duty and heavy-duty repair clamps may be used. Heavy-duty clamps used to secure high-pressure pipes consist of two cylindrical half shells that will be bolted around the pipe (Figure 2.3). Medium-duty clamps used for low pressure applications may be made as a single piece, with a flexible region, allowing it to conform to the shape of the pipe. These types of clamps totally enclose and seal the

defective area with elastomeric seals at the inside face of the clamps. As the clamps are tightened, the compression forces may allow for a tighter seal.

Similar to bolted clamps, encircling sleeves consisting of two cylindrical halves that conform to the geometry of the pipe when welded together longitudinally is a simple method to reinforce a defective section of a pipe. For pressure applications, the encircling sleeves must be fully seal-welded to the pipe.

A more advanced version of the encircling sleeves consists of using split-sleeves with epoxy-grout in the middle. This method allows for the use of a fast curing polyester based resin seal to affix the sleeve onto the pipe instead of sealing through welding. This repair method is still capable of withstanding high circumferential and axial stresses; furthermore, it is capable of withstanding on-going internal metal loss even if the extent of the corrosion advances through the pipe wall. The epoxy grout transfers the stresses from the pipe substrate to the steel repair sleeve, thereby confining the steel pipe and preventing the damaged area from radially expanding outward. The use of epoxy grout introduces limitations such as operating pressure which is limited to approximately 1450 psi and temperature which ranges between 3^{o}C and 100^{o}C. This is not a rapid repair method as the two cylindrical sleeve-halves are required to be welded together, and the epoxy needs approximately 24 hours to cure to 90% of its ultimate strength (AEA Technology Consulting, 2001).

2.5 Composite Repair Systems

While conventional steel repair techniques have been effective, recently composite repair systems have been gaining popularity since composite repairs have an advantage over

clamps as they are not constrained by length or complex geometry; and when compared to welding, since no hot work is required composite repairs are safe even when applied while the pipeline is operational. Other benefits of fibre composites include their manoeuvrability, ease of use in tight spaces and low density, allowing FRP (Fibre Reinforce Polymer) repairs to restore structural strength without significantly increasing the self-weight of the structure. Pipeline repair using FRP began in the late 1980s. After continuous development of FRP composite systems, there are now a few different options available in the market for pipe repair using composite FRP systems. FRP composites can be categorized as pre-cured layered systems, flexible wet lay-up systems, and pre-impregnated systems (Lim et. al , 2015).

Flexible Wet Lay-up systems use a fabric FRP that is flexible before curing. In order to apply this repair technique, voids and corroded areas are cleaned and filled in with putty. Then an epoxy resin is applied on the pipe substrate and the FRP fabric is wrapped around the pipeline while the fabric is also coated with the epoxy resin (Figure 2.4). After curing, the wrap becomes extremely rigid. This method has an advantage over using steel repair techniques because it can be applied on bends and joints. However, as stated by Lim et al. (2015) there could be problems with the in-situ curing process when done in the field, due to high ground water table. Also the application of this system may be difficult in confined spaces.

Pre-cured layered systems are factory-manufactured with layers of FRP composites bonded together with a strong adhesive. It coils as cured in order to fit a pipe's geometry. Since it is pre-manufactured, better quality control can be expected than the wet lay-up system. However, due to the stiffness of pre-cured systems they cannot be applied on

bends and joints. Similar to the wet lay-up system, during application, the corroded area is filled with infill material and the pre-cured FRP composites are attached to the pipe using adhesive (Lim et al., 2015).

The pre-impregnated system is a mix of the wet lay-up and pre-cured systems as fibres are coated with a matrix material (epoxy) and partially cured in a controlled, factory setting. Since the fibres are only partially cured they are still flexible at the time of application. However, they need to be stored in a cold environment to prevent full curing. ProAssure Wrap Extreme, a pre-impregnated composite repair system, is suitable for both onshore and offshore applications. It is made of E-glass fibre with an epoxy that is capable of curing underwater with minimal loss of adhesion and mechanical properties (Lim et al., 2015).

In order to validate the effectiveness of composite repair systems many researchers have conducted experimental work involving pipes with simulated corrosion. Chan et. al (2014) used a pre-cured layered system to repair a corroded section of pipe. An API 5L X52 pipe was machined to reduce the wall thickness by 50% to simulate corrosion. The length of the corrosion patch was 622 mm in the axial direction and covers the full circumference. The purpose of the investigation was to see if the burst pressure of the machined pipe could be increased with the use of Helicoid Epoxy Sleeve (HES) composite repair system. The HES system uses carbon fibre for reinforcement with epoxy grout being used as the fill material. Burst pressure of the pipe was calculated according to American Bureau of Shipping standard, a guide for building and classing subsea riser system:

$$P_b = 0.90(SMYS + SMTS)\left(\frac{t}{D_0 - t}\right) \quad (2.2)$$

The thickness of the laminate needed for repair is based on the ASME PCC-2, Short-term Pipe Spool Survival Test (Appendix III) guidelines. Two layers of 0.8mm thick carbon FRP strips were used to satisfy repair thickness of 1.08 mm.

It was found through numerical analysis that the use of the HES system increased the burst strength of the corroded pipe by 124% at the design pressure (Figure 2.5). The experimental results and FEA analysis confirmed an increase in the burst strength of the corroded pipe beyond that of the uncorroded pipe (Chan et al., 2014).

M. Elchalakani (2016) conducted 3-point bending tests on steel tubes to investigate the bending behaviour of circular hollow sections, both corroded and repaired using carbon FRP (CFRP) fabric. The corrosion in the CHS was simulated by machining 20%, 40%, 60%, and 80% off of the wall thickness over the entire circumference. No internal pressure was applied on the CHS for the tests. Two types of composite wraps were used for the repair: Structural Technology V-Wrap C200 and Sika-Wrap 300-C. 31 specimens with a diameter of 101.6 mm and thickness of 5.0 mm were tested. The study found that all the repaired CHS saw a large increase in strength, with a maximum of 282% for one of the 80% corroded specimen. The average increase in strength of the corroded CHS was 97%. However, none of the specimens were able to revert back to the original, uncorroded strength, except for the 20 % corrosion specimen with two layers of wrap (Figure 2.6).

Shouman and Taheri (2009) conducted FEM analysis on corroded pipe sections subjected to internal pressure and bending. For the repair of the pipe, the Clock Spring composite

wrap system, which uses E-glass, was modelled around a defect of 80% of the wall thickness. It was found that a corroded pipe that has been retrofitted with the Clock Spring composite wrap can outperform the virgin pipe section.

2.6 Codes and Standards

As more research is being conducted on the use of FRP systems to repair corroded pipes, many codes and standards have adopted guidelines to assess the remaining strength of the corroded pipe sections and repair them.

2.6.1 ASME B31G

A popular guideline used to measure the remaining strength of corroded pipes is the ASME B31G manual. In the 1991 version of the ASME B31G manual, the depth of a corrosion pit is calculated as relative to the nominal uncorroded wall thickness as a percent: $\%\, pit\ depth = 100d/t$. The maximum allowable longitudinal length of the corroded area is determined by the equation:

$$L = 1.12B\sqrt{Dt}. \tag{2.3}$$

The value of the constant B is determined by:

$$B = \sqrt{\left(\frac{d/t}{1.1\frac{d}{t}-0.15}\right)^2 - 1} \tag{2.4}$$

In the above equation the value of B must not exceed 4, unless the corrosion depth is between 10% - 17.5%, in which case the value of B is 4. A pipe with a maximum

corrosion depth of 10-80% of the nominal wall thickness should not have a corrosion patch longer than L, calculated in Equation 2.3.

Based on the above equations, a few tables have been formed in the ASME B31G standard that allows the reader to quickly establish an estimate of the maximum corrosion length, depending on the diameter, wall thickness and maximum corrosion depth of the pipe.

If the length of corrosion is greater than the calculated value of L, and the depth of corrosion is 10 - 80% of the wall thickness, the ASME B31G recommends repairing the corroded section or lowering the maximum allowable operating pressure (MAOP) to P' or below, where P' is the maximum pressure that is determined to be safe for the corroded section.

The value of P' depends on the factor A_1, which compares the length of longitudinal corrosion to the pipe's diameter and thickness:

$$A_1 = 0.893\left(L_m/\sqrt{Dt}\right) \tag{2.5}$$

If A_1 is less than or equal to 4, P' is calculated as:

$$P' = 1.1P\left[\frac{1-\frac{2}{3}\left(d/t\right)}{1-\frac{2}{3}\left(\frac{d}{t\sqrt{A_1^2+1}}\right)}\right] \tag{2.6}$$

Where P is the greater of either the MAOP or $P = \frac{2StF}{D}$. F is a design factor from ASME B31.4, ASME B31.8, ASME B31.11. The value of F is normally taken as 0.72 (Pipelines and Risers, 2001). If A_1 is greater than 4, P' is calculated as :

$$P' = 1.1P\left[1 - {}^{d}/_{t}\right] \tag{2.7}$$

The ASME B31G document has gone through heavy revisions since the first issue in 1984, in order to incorporate other, newer methods of corrosion evaluation that have been proven reliable. Depending on the data available and the data needed, the 2009 revision of the document provides four levels of analysis to evaluate the conditions of the pipe, ranging from Level 0 to Level 3. A Level 0 evaluation is the most basic level of analysis, where the diameter and thickness of the pipe is used with the maximum depth of corrosion to find the maximum allowable length of corrosion or vice versa from a set of tables. If the actual length of corrosion on the pipe is lower than the table, the metal loss area is deemed acceptable. Level 1 evaluation is used to determine whether the operating pressure of the pipe is acceptable with the given metal loss area. The estimated failure stress level of the pipe, S_F, is mainly dependent upon the bulging stress magnification factor, M, and flow stress, S_{flow}. As stated in the code, "flow stress is not a property specified in a material grade or finished product standard". Instead, the code provides three equations to define the flow stress, based on the operating temperature and SMYS in paragraph 1.7(b).

$$S_{flow} = 1.1\ x\ SMYS \tag{2.8}$$

when operating temperature is below 250^{o}F

$$S_{flow} = SMYS + 70\ ksi\ (69\ MPa) \tag{2.9}$$

when SMYS is 70ksi or less and operating temperature is below 250^{o}F

In the 2009 version of the ASME B31G code, the bulging stress magnification factor, M, is defined as:

$$M=\left(1+0.6275z-0.003375z^2\right)^{1/2} \tag{2.10}$$

for $z \leq 50$, and

$$M=0.032z+3.3 \tag{2.11}$$

for $z > 50$, where

$$z=L^2/Dt \tag{2.12}$$

Using the provided bulging stress magnification factor, the estimated failure stress level of the pipe, S_F, can be determined using the equation:

$$S_F = S_{flow}\left[\frac{1-0.85(d/t)}{1-0.85(d/t)/M}\right] \tag{2.13}$$

If the failure stress is greater than the hoop stress multiplied by an acceptable factor of safety, the flaw is deemed acceptable. It is important to note that this standard does not consider the effect of axial stresses on pipe defects.

Level 2 evaluation is also used to determine the failure stress of the pipeline; however, it is performed using the Effective Area Method. In this case the approximation of the defect area has been changed when calculating the failure stress, S_F:

$$S_F = S_{flow}\left[\frac{1-A/A_0}{1-(A/A_0)/M}\right] \tag{2.14}$$

A=effective area of missing metal

A_0=original area

Several measurements need to be taken along the metal loss area in order to use the Effective Area Method as it needs a detailed profile of the corrosion along the longitudinal direction of the pipe. This is an iterative method that examines all possible combinations of local metal loss with respect to the original material. The number of iterations is determined by:

$$n!/2(n-2)! \tag{2.15}$$

n = number of measurements taken

A Level 3 evaluation is the most complex of the four as it involves finite element modelling of the corroded region. In order to get an accurate result, the loadings, boundary conditions, ovality, material properties of the pipe, along with many other factors affecting the pipe have to be modelled correctly. However, since the model is made specifically for the pipe, the results will be more accurate than the previous three methods.

2.6.2 ASME PCC-2

ASME PCC-2 is a standard that provides guidance on the matter of repairing pressure equipment and piping. Once the pressure equipment has been properly inspected and it is determined that repairs are necessary, the technical procedures and information provided in this standard can be used to conduct necessary repairs. The repair information provided

in the standard cover methods involving metal deposits, such as welding or soldering, methods involving mechanical repairs including bolted clamps, and methods involving non-metallic composite repair systems.

For composite repairs, the standard considers two design cases: Type A, where the pipe does not leak and only needs structural reinforcement and Type B, where the pipe needs structural reinforcement and sealing of leak.

For pipe systems, where the underlying substrate does not yield, the minimum thickness needed to support the hoop stress due to internal pressure is calculated by:

$$t_{min} = \frac{D}{2s} \cdot \left(\frac{E_s}{E_c}\right) \cdot (P - P_s) \tag{2.16}$$

For pipe systems, where the underlying substrate does not yield, the minimum thickness needed to support the axial stresses due to bending or other axial loads is calculated by:

$$t_{min} = \frac{D}{2s} \cdot \left(\frac{E_s}{E_c}\right) \cdot \left(\frac{2F_a}{\pi D^2} - P_s\right) \tag{2.17}$$

The ASME PCC-2 code states that the value of F_a, the sum of axial tensile loads, shall be determined by the repair system designer, and is outside the scope of the article.

For pipe systems, where the underlying substrate does yield, the laminate thickness is designed based on the allowable strain of the composite. The minimum thickness needed to support the hoop stress due to internal pressure is calculated iteratively by:

$$\varepsilon_c = \frac{PD}{2E_c t_{repair}} - s\frac{t_s}{E_c t_{repair}} - \frac{P_{live} D}{2\left(E_c t_{repair} + E_s t_s\right)} \tag{2.18}$$

If the internal pressure during the application of the repair is zero, the equation can be rearranged to:

$$t_{repair} = \frac{1}{\varepsilon_c E_c}\left(\frac{PD}{2} - st_s\right) \tag{2.19}$$

According to the code, when determining the design repair laminate thickness for pipes where the underlying substrate is assumed to have yielded, only hoop loading should be considered.

If the remaining strength of the original pipe is to be ignored in the determination of the load-carrying capacity, the code recommends the following equations to design the repair laminate thickness to bear the hoop stresses:

$$t_{min} = \frac{1}{\varepsilon_c}\left(\frac{PD}{2}\,\frac{1}{E_c} - \frac{F_a}{\pi D}\,\frac{\upsilon_{ca}}{E_c}\right) \tag{2.20}$$

and axial stresses:

$$t_{min} = \frac{1}{\varepsilon_a}\left(\frac{F_a}{\pi D}\,\frac{1}{E_a} - \frac{PD}{2}\,\frac{\upsilon_{ca}}{E_c}\right) \tag{2.21}$$

These two equations are temperature dependant as ϵ_a andϵ_a, the allowable repair laminate strains, are calculated based on temperature factor,f_T, temperature difference between operation and installation, ΔT, and thermal expansion coefficients, α_s and α_c.

ASME PCC-2 recommends using Type B repairs if a pipe is leaking or the substrate at any point is determined to be less than 1 mm at the end of its life. For circular defects or

noncircular defects that have an aspect ratio less than 5 the repair laminate thickness is found through iteration of the equation:

$$P = f_T f \sqrt{\frac{\gamma}{\frac{(1-\upsilon^2)}{E}\left(\frac{3}{512t_{min}^3}d^4 + \frac{1}{\pi}d\right) + \frac{3}{64Gt_{min}}d^2}} \tag{2.22}$$

For rectangular type defects where the width, W, satisfies the condition $\leq 1.65\sqrt{Dt_{min}}$, the repair laminate thickness is found through iteration of the equation:

$$P = f_T f \sqrt{\frac{\gamma}{\frac{(1-\upsilon^2)}{E}\left(\frac{1}{24t_{min}^3}W^4 + \frac{\pi}{4}W\right) + \frac{3}{16Gt_{min}}\frac{\left(\frac{4}{5}+\frac{\upsilon}{2}\right)}{1+\upsilon}W^2}} \tag{2.23}$$

If the repair thickness of the laminate is governed by axial loads, the code requires that the ends of the repair are tapered. For non-leaking repairs, it is also required to provide an overlap length of:

$$L_{over} = 2.5\sqrt{Dt/2} \tag{2.24}$$

Consequently the minimum axial length of repair will be

$$L_{repair} = 2L_{over} + L_{defect} + 2L_{taper}. \tag{2.25}$$

2.6.3 ISO/TS 24817

The ISO/TS 24817 standard, published in 2006, also provides guidelines on composite repair of pipelines, so that the repaired pipelines may achieve an acceptable level of strength to withstand the loadings and conditions they face. The repair guidelines provided in this standard covers external corrosion, internal corrosion, pitting, circumferential cracks, and through-wall penetration. The approach used in this standard is much the same as the ASME PCC-2 standard. The equations for determining the repair thickness of the laminates are the same as those used in the ASME PCC-2 standard. However, the ISO standard offers an equation to find the equivalent axial load that is not provided in the ASME standard:

$$F_{eq} = \frac{\pi}{4} pD^2 + \sqrt{F_{ax}^2 + 4F_{sh}^2} + \frac{4}{D}\sqrt{M_{ax}^2 + M_{to}^2} \tag{2.25}$$

2.6.4 CSA Z662

CSA Z662 is the standard provided by the Canadian Standard Association regarding oil and gas pipelines. It provides guidance on all aspects of the life of the pipeline, including design, operation, maintenance, deactivation, and abandonment. Regarding the use of composites for the repair of pipelines, the CSA Z662 standard contains two sections that discuss the use of composite reinforcement repair sleeves and fibre-reinforced composites.

The CSA standard requires composite repair sleeves to conform to the requirements of ASME PCC-2, Article 4.1 or ISO/TS 24817. It also requires the repair sleeve and the remaining pipe wall to have a load-carrying capacity that is at least equal to the original

pipe without corrosion. If the internal corrosion has been arrested, the repair sleeve may be used as a permanent repair for the pipe.

A composite-reinforced steel pipe is defined by the CSA Z662 as a steel pipe reinforced by fibre-reinforced composite material which shares the functional circumferential loads with the steel pipe. A formula is provided in the standard to calculate the design pressure of a composite-reinforced steel pipe. The formula is a modified version of Barlow's equation which takes into account the thickness along with the strength of the composite in the hoop direction.

$$P = \frac{2}{D} \times (stT + T_h w) \times F \times L \tag{2.26}$$

According to the standard, the fibres used for the composite shall consist only of glass fibres.

2.7 Summary

From the literature review, it is evident that CFRP and GFRP are effective at increasing the burst strength of corroded pipes. No studies have been found that use basalt FRP composites to reinforce pipes for any type of loading. While there is a lot of literature focused on burst pressure, only two studies were found that analyzed the effect of using FRPs on pipes subject to bending. Shouman and Taheri (2009) proved that a highly corroded pipe retrofitted with the ClockSpring repair sleeve made of GFRP can outperform the virgin pipe in bending capacity. Elchalakani (2016) showed that the carbon wrap is able to increase the load carrying capacity. However, the repair using CFRP was only able to repair a specimen with corrosion measuring 20% of the wall

thickness to its uncorroded state. The author does not mention encountering a wrinkle defect in any of his specimen, probably due to the fact that the tubes were used were unpressurized.

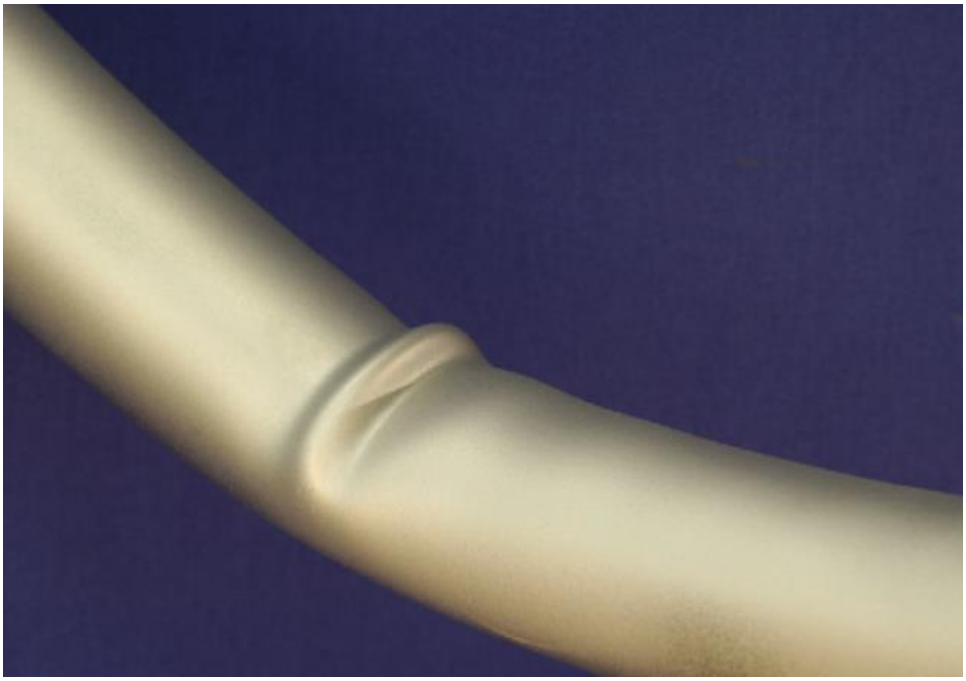

Figure 2.1: Local buckling due to wrinkle in pressurized tube (Limam et al., 2010)

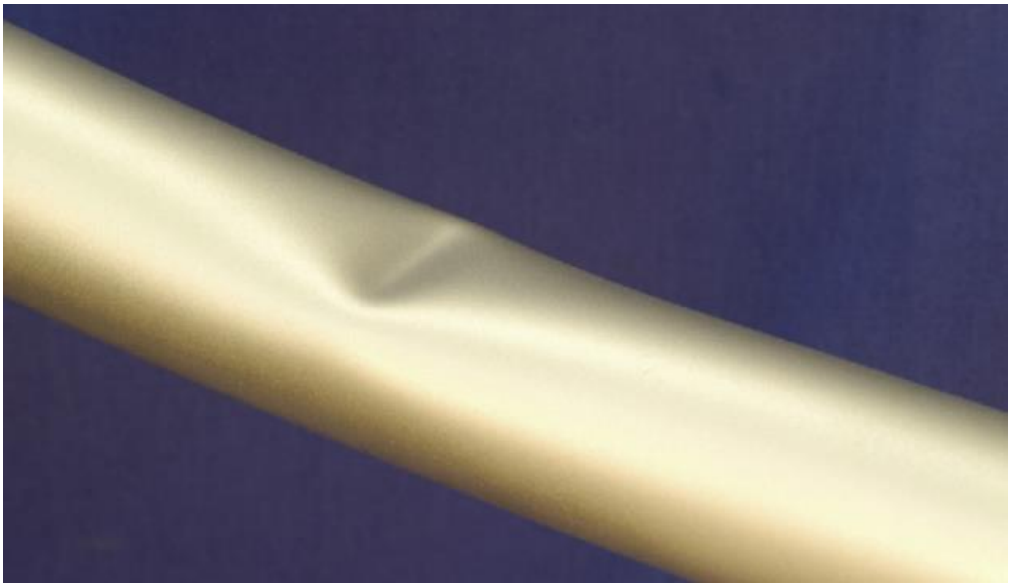

Figure 2.2: Local buckling due to kink defect in unpressurized tube (Limam et al., 2010)

Figure 2.3: Heavy duty clamps used for the repair of high integrity applications (AEA Technology Consulting, 2001)

Figure 2.4: Application of the wet lay-up system (Duell, Wilson, & Kessler, 2008)

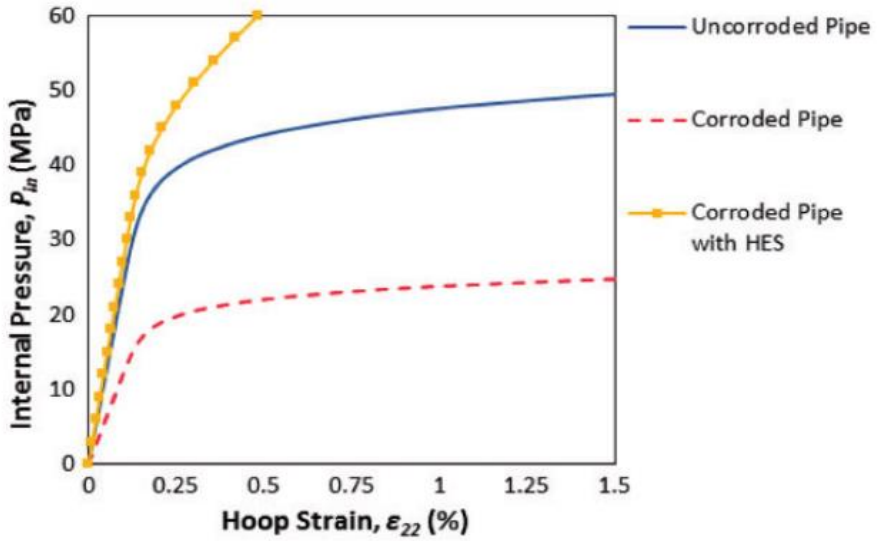

Figure 2.5: Internal pressure vs. hoop strain curves for pipe specimens tested for burst pressure (Chan et al., 2014)

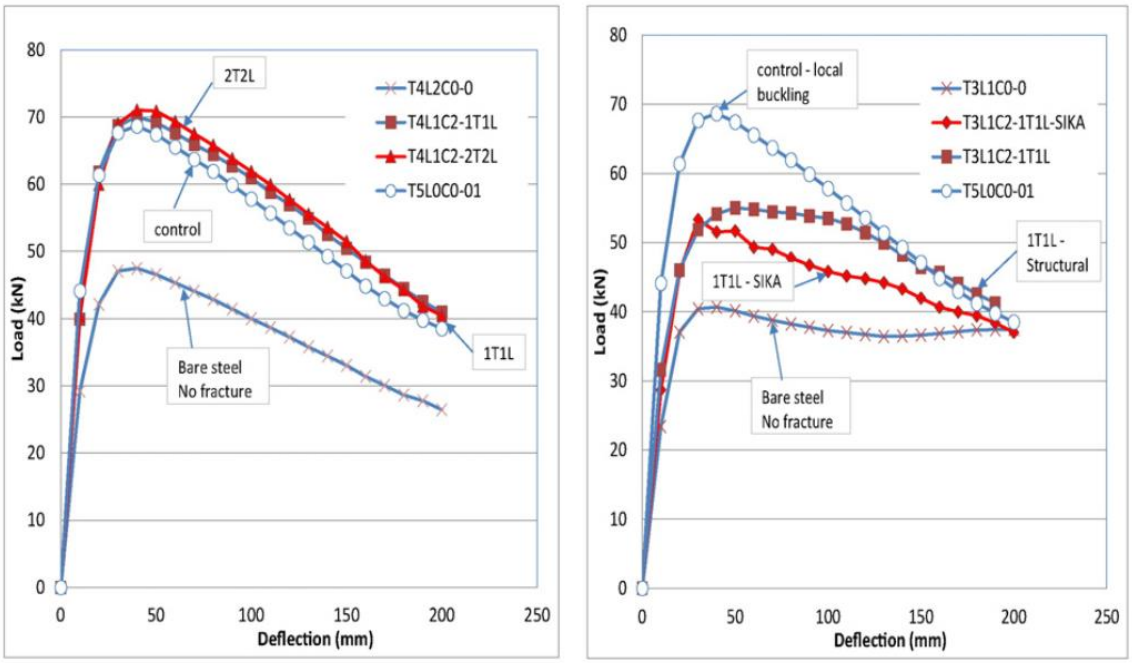

20% corrosion

40% corrosion

Figure 2.6: Comparison of control specimen with corroded and CFRP-repaired specimens of 20% and 40% corrosion (Elchalakani, 2016)

Chapter 3 Experimental Program

The objective of this research is to determine whether BFRP composites are able to restore the load-carrying capacity of a corroded pipe to its uncorroded state and if the composite is able to change the buckling mode of pipes subjected to bending and stop the wrinkling process. As discussed in the literature review, much of the research that has been done studied the effect of Fibre Reinforced Polymers (FRPs) on the burst strength of corroded pipes. A study, conducted by Elchalakani (2016), was found that analyzed the effects of lateral loads on FRP-repaired pipes with simulated corrosion. However, it is important to note that the tests conducted by Elchalakani used unpressurized pipes under 3-point bending. The studies conducted by Ju and Kvriakides (1991) indicated that unpressurized pipes do not develop a wrinkle and instead buckle with a kink defect. Therefore, it was important to note that the current project used pressurized pipes to study the wrinkle behaviour.

The test setup used by Elchalakani (2016) used the three-point bending test configuration. However, the three-point bending test subjects only the section directly under the loading point to the maximum stress and maximum moment. In the four-point bending test, however, the maximum stress and maximum moment are distributed in the area between the two loading points; as a result more of the flaws in the material will be exposed to the maximum stress. Therefore, the strength obtained from the three-point flexural test are expected to be much higher than that obtained from the four-point bending test (ASTM, 2017).

It was decided to conduct five full-scale experiments for this research to verify whether or not basalt fibre reinforced polymer (BFRP) is capable of restoring the load-capacity of corroded pipes to their uncorroded state while bending. Table 3.1 shows the test matrix used in this study. The first test was performed on an uncorroded pipe specimen in order to establish a reference for the bending performance. The second and fourth specimens were machined with defects of depths of 1.2 mm (20% of the wall thickness) and 2.4 mm (40% of the wall thickness), respectively (Figure 3.1). These two tests were used to determine the effect of two corrosion depths, and to make a relative comparison to the repaired specimens. Similar to the second and fourth specimens, the third and fifth specimens were also machined with defects of the same depth. However, before testing, specimens 3 and 5 were retrofitted with ten and twenty layers of uniaxial BFRP wrap respectively. The purpose of specimens 3 and 5 was to observe whether the performance of the corroded pipe improved, relative to the unrepaired pipe.

Table 3.1: Test Matrix

Specimen No.	Corrosion on pipe wall	Number of layers of BFRP
1	0	0
2	20%	0
3	20%	10
4	40%	0
5	40%	20

3.1 Instrumentation

Data Acquisition System

A computerised data acquisition system was used to collect the data transmitted by the strain gages, Linear Variable Differential Transformer (LVDTs), inclinometers, and pressure transducer. Two NI-9235 bridge input modules with 8 channels each were used to collect the strain gage data. Collected data from all the connected instruments was processed using LabVIEW software, which takes the strain and voltage readings and converts them into usable information using calibration factors. The software was programmed to store one reading per second.

Strain Gages

A strain gage is a tool used to measure the strain in a localized area of an object. Kyowa strain gages of type KFG-5-120-C1-11 were used to measure the strain in the critical areas of the pipe. The strain gages are made of a polymide resin base and a copper-nickel alloy grid measuring 5 mm by 1.4 mm. Hence, the gauge length of the strain gage is 5 mm.

The strain gages were attached to the surface of the pipe using Loctite 401 instant adhesive. As the pipe section deforms the conductive metal grid stretches or compresses accordingly. As the metallic grid becomes longer and narrower or shorter and broader, the resistance of the strain gage also changes. The strain is determined from the measured electrical resistance of the strain gage.

Linear Variable Differential Transformer

LVDTs are used to measure linear displacement. The internal structure of an LVDT consists of three solenoids, with the primary solenoid in the middle and two secondary solenoids placed equidistant from the primary solenoid at each end. The primary solenoid is exposed to an Alternating Current (AC) of constant magnitude, which creates a magnetic flux and produces voltages in the secondary solenoids. There is a magnetic core at the center of the three solenoids, attached to a wand that extends past stainless steel housing. The extended part of the wand is attached to the object whose displacement is to be measured. As the object moves, the wand also moves linearly, pushing or pulling the attached core through the solenoids. As the core moves closer towards either secondary solenoid, more flux is coupled to the closer solenoid and less flux is coupled to the other secondary solenoid. The difference between the voltages of the secondary solenoids is the output given by the LVDT. The data acquisition system multiplies the output given by the LVDT with a calibration factor in order to determine the linear displacement.

Inclinometers

Two inclinometers were placed on the top of the pipe at each end and secured in place using stainless steel bands. The inclinometers were used to measure the amount of rotation the pipe was subjected to near the supports.

Pressure Pump

A P300 series hydrostatic pump by BARBEE Engineered Testing Systems was used to pressurize the pipe. The valves at the rear take in water and pressurized air, and pumps

out pressurized water. The hydrostatic pump was used to increase the pressure inside the pipe to 850 psi.

Collars

In order to ensure that the wrinkle does not occur near the supports due to the large stress concentration in that area, six collars were placed on the pipe. The collars can be seen in Figure 3.7 and 3.10. Each collar was made by cutting off a ring approximately 40 mm in width from the pipe. Each ring was then cut into two semi-circular halves and each end was welded with a punctured steel angle, making one collar. In order to tighten the collars, the holes on angles on each collar was aligned and fastened with a bolt and screw.

Hydraulic Jack

The jack consists of a tension-compression loading plunger cylinder equipped with a load cell by AEP Transducers to measure the applied load. The cylinder is able to exert both push and pull forces, in order to create tension and compression as needed. The load transducer is used to measure compression loads up to 3 MN and tension loads up to 2.5 MN.

The cylinder is operated by a ZE4440SB hydraulic electric pump by Enerpac. The hydraulic pump is able to move the piston in the cylinder up or down by increasing or decreasing the pressure.

3.2 Material Properties

Five pipe specimens were cut at approximately 2120 mm length from two long pipe sections taken from the same linepipe. The specimens had an outer diameter of 219 mm

(8.625 inches) and thickness of 6.35 mm (0.25 inches), indicating that the pipe is a NPS 8, Schedule 20 pipe. The diameter-to-thickness (D/t) ratio of the pipe is 34.5.

In order to determine mechanical properties of the material such as yield strength, tensile strength and elastic modulus, coupon tests were conducted using the ASTM E8/E8M-09 (ASTM, 2010) standard. Four coupons were cut from the pipe in the longitudinal direction, away from the weld seam. The coupons were mounted with a 50 mm gage length extensometer and subjected to uniaxial tensile stress until rupture (Figure 3.2 and 3.3). The load values from the built-in loadcell of the testing machine and strain values from the extensometer were recorded by LabVIEW. The engineering stress was determined by dividing the load values from the original area.

The tensile properties of the basalt FRP composites were obtained by eight coupon tests based on the ASTM D3039/D3039-14 (ASTM, 2015) standard to determine the rupture strength, rupture strain and elastic modulus of the composite. The compressive and shear properties of the BFRP composites were found by testing coupon specimens and analyzing the results using Digital Image Correlation, in collaboration with Amirreza Bastani (Figures 3.4, 3.5).

3.3 Test Setup

The hydraulic jack was vertically aligned and bolted on to a large steel reaction frame. Two large steel stands were bolted to the floor approximately 2500 mm away from each other, with the hydraulic jack at the center.

Each pipe specimen was cut to approximately 2120 mm, and steel plates were welded onto each end. The end plates were first drilled and threaded in order to be able to

connect fittings at either end. Next, the end caps were fitted with valves, in order for the pipe to be filled with water. When filling the pipe, it was lifted vertically into the air so that all air in the pipe would be expelled from the pipe when it is filled with water (Figure 3.6). Afterwards, a grinder was used to grind off the rust and polish a strip of the middle portion of the pipe in order to attach strain gages. For each pipe, several strain gages were attached using Loctite 401 glue where the wrinkle was expected to occur (Figure 3.7).

The test setup allows the supports to rotate in one direction using a custom-made mechanism with two protruding cylinders with balled ends, similar to a large ball stud. When the half-cylindrical holes on the underside of the supports rest on the balled ends of the mechanism, a hinge is created, allowing the supports to freely rotate in a single direction. The balled ends of the bottom support were screwed on to the large steel stands and the balled ends of the top support were screwed on to the underside of the spreader beam.

Once the bottom supports were in place the pipe was lowered on to the supports. For specimens with simulated corrosion, the placement of the pipe was adjusted so that the corrosion patch was directly underneath the loading jack and facing upwards. A hose connected to the pressure pump was attached to one end of the pipe and a pressure transducer was attached to the other end.

Next, the top supports were placed on the pipe at a center-to-center distance of 500 mm. The balled ends of the top support that were screwed on to the spreader beam were lowered into the semi-cylindrical holes of the top supports. Similar to the bottom

supports, this setup allows the top supports to rotate in the direction of the length of the pipe.

Six collars were placed on the pipe, two on the outside edge and one on the inside edge of each top support to stop the formation of a wrinkle at the supports. Next, two inclinometers were placed at each end of the pipe, directly above the bottom supports, to measure the curvature as the pipe bends. LVDTs were placed under the pipe and on the loading jack to measure the amount of deflection that the pipe specimen experienced. The hydraulic jack was lowered until it made contact with the spreader beam (Figures 3.8, Figure 3.9).

3.4 Test Procedure

Once the setup was completed, all the data collection instruments were connected to the data acquisition system. Before starting the test, all values were set to zero, and the hydrostatic pump was used to raise the pressure inside the pipe to 20% of the yield stress, 5.86 MPa (850 psi). Once all the preparations were complete, load was slowly applied and increased using displacement control method. The hydrostatic pump was manually adjusted throughout the test to keep the pressure at nearly 5.86 MPa (850 psi).

Loading was continued until it could be seen that a wrinkle formed (Figure 3.10). At that point, the pipe specimen was unloaded and the collars were removed. Afterwards, load was reapplied past the previous point in order to obtain a fully developed wrinkle of desired shape with target value of displacement in the load-displacement curve (Figure 3.11).

3.5 Corrosion Repair

Pipe specimens 3 and 5, with corrosion of 20% and 40% of the thickness respectively, were repaired using BFRP (Table 3.1). The repair process was conducted before placing the pipe on the supports. After the pipe was filled with water one strain gage was attached at the middle in the longitudinal direction of the pipe for specimen 3. For specimen 5, three strain gages were attached. A small piece of wire, approximately three-inches in length was soldered onto each strain gage.

Basalt Fabric

The repair process involved attaching several layers of basalt fabric onto the substrate of the pipe to compensate for the thickness lost due to corrosion. Ten layers of fabric were used for the repair of specimen 3 and twenty layers of fabric were used for the repair of specimen 5 (Table 3.1). As stated in the literature review, ASME PCC-2 (ASME, 2015) recommends an axial repair length of:

$$L = 2L_{over} + L_{defect} + 2L_{taper} \tag{3.1}$$

where L is the total length of repair, L_{over} is the overlap length, L_{defect} is the defect length, and L_{taper} is the length of the taper

The recommended axial length of repair by ASME PCC-2 is 227 mm. The axial length of each layer was tapered from 350 mm for the bottom layer to 314 mm for the top layer. The uniaxial fabric was applied with the fibres aligned in the longitudinal direction of the pipe in order to carry the axial compressive stresses of the pipe when subjected to bending.

Square pieces of basalt fabric were used as the filler material to fill in the corrosion patch. Specimen 3 with 20% corrosion used three layers measuring 75 x 75 mm, 85 x 85 mm, and 95 x 95 mm. Specimen 5 with 40% corrosion used five layers measuring 75 x 75 mm, 80 x 80 mm, 85 x 85 mm, 90 x 90 mm, and 95 x 95 mm.

Application of FRP

Before attaching the BFRP onto the pipe, a grinder was used to clean the pipe substrate of all dirt and rust. The surface was wiped clean using acetone. MasterBrace P 3500 type primer was used to prepare the surface before applying the resin. The two-part primer was mixed at the recommended ratio of 100 Part A to 60 part B by weight. A roller was used to apply the primer on to the substrate.

After the primer had fully cured, the repair process began. The epoxy, MasterBrace SAT 4500, was mixed at a ratio of 100 part A to 30 part B by weight. A roller was used to completely cover the primed surface with epoxy. Then each of the square layers of fabric used for the filler was placed in the corrosion patch starting from the 75 x 75 mm layer. When placing the fabrics, the small wire soldered to each strain gage on the corrosion patch was weaved through the fibres of each layer. After applying each layer, that layer was completely saturated with epoxy (Figure 3.12, Figure 3.13).

3.6 Summary

In summary, this section discusses the specimen preparation, instrumentation and test setup and the repair process that was used to conduct the laboratory experiments.

Figure 3.1: Specimen 2, with 1.2 mm (20% wall thickness) deep corrosion patch

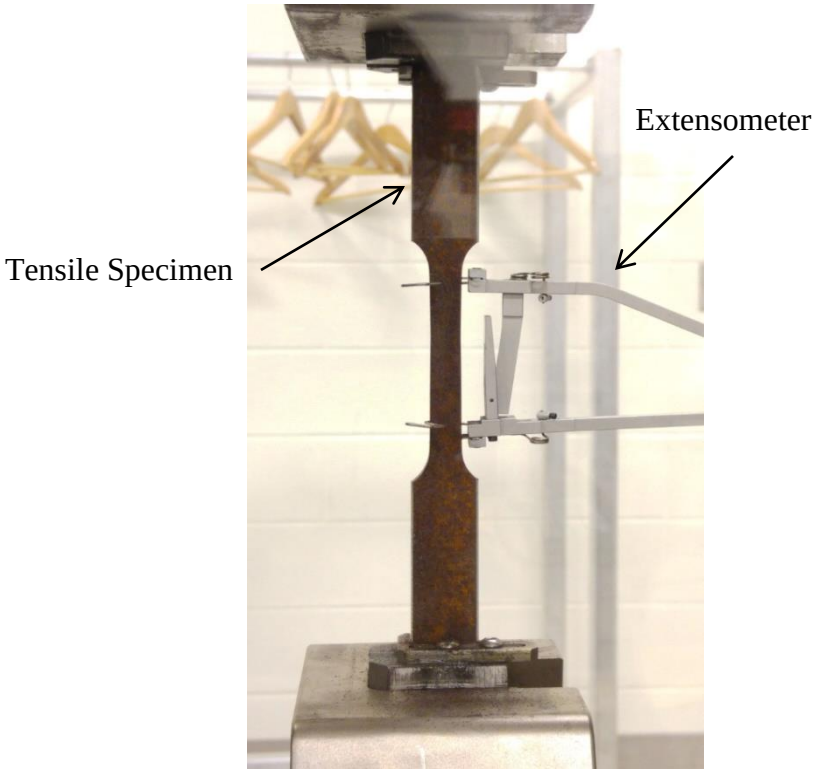

Figure 3.2: Steel coupon from pipe under uniaxial tension test

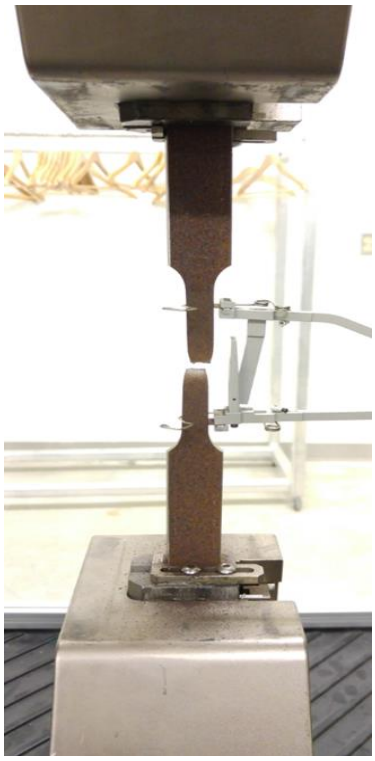

Figure 3.3: Rupture of steel coupon from pipe specimen

Figure 3.4: Testing of a BFRP coupon in shear

Figure 3.5: Ruptured BFRP coupon specimens after testing

Figure 3.6: Filling specimen 3 with water

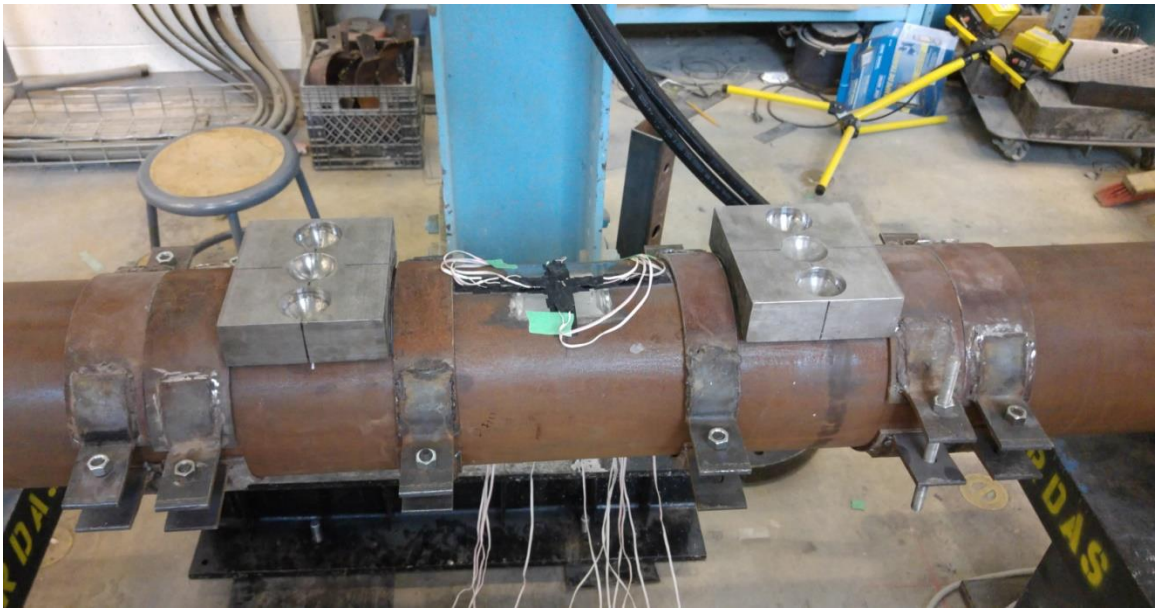

Figure 3.7: Strain gages attached to the corrosion patch of specimen 2

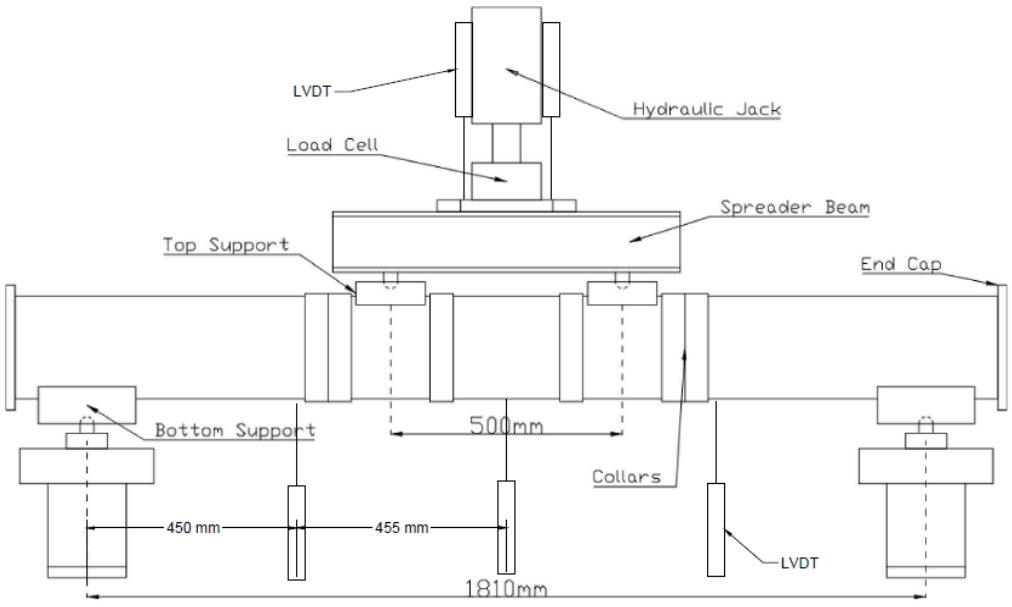

Figure 3.8: Schematic of the test setup

Figure 3.9: Test Setup

Figure 3.10: Initiation of wrinkle

Figure 3.11: Fully developed wrinkle

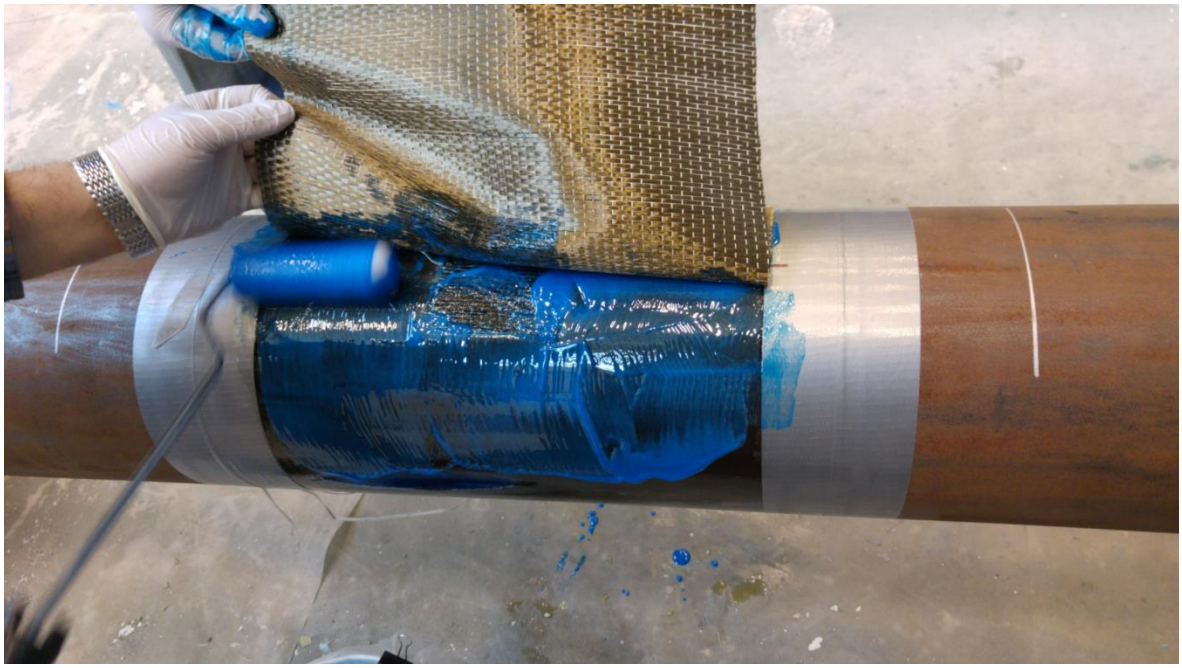

Figure 3.12: Application of basalt fabric onto the epoxy-wetted surface

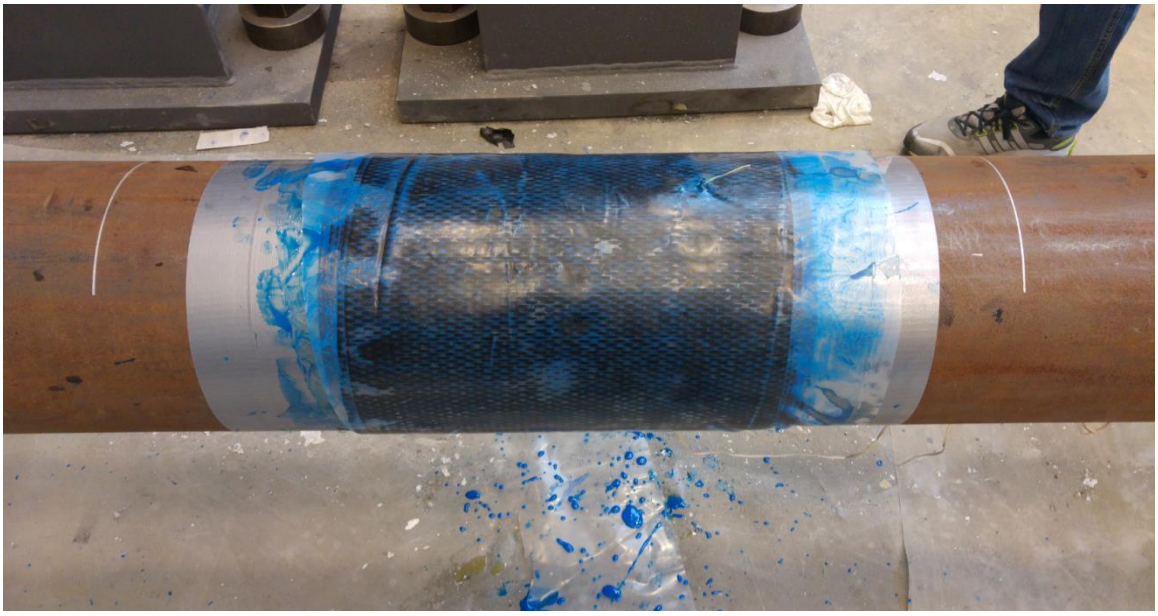

Figure 3.13: Specimen 3 after applying ten layers of basalt fabric and epoxy

Chapter 4 Experimental Results

As discussed in the previous chapters, the objective of this research is to determine how BFRP wrap affects the buckling process of a corroded pipe when subjected to bending. Five full-scale pipe specimens were tested under four-point bending to accomplish this goal. The test matrix is shown in Table 3.1. The test parameters and results are shown in Table 4.1

4.1 Test 1

Specimen 1 was used to determine the behaviour of an undamaged pipe when subjected to bending. Load was applied until a noticeably large wrinkle formed.

The specimen reached an ultimate load of 412 kN, showing initiation of global yielding at a load of approximately 300 kN. The formation of a wrinkle was noticed at a displacement of 56 mm and a load of 407 kN, at which point the specimen was unloaded and the collars were removed. It was found that the wrinkle developed approximately 25 mm off-center. The specimen was reloaded until a displacement of 90 mm, in order for the wrinkle to grow and to get a better representation of the load-deformation behaviour. The load-deformation behaviour of Specimen 1 is illustrated in Figure 4.3.

It was expected that the wrinkle would occur at the middle of the pipe. However, the wrinkle formed near the inside of the collars due to the localized stress concentration in that area, with one foot of the wrinkle ending at the center of the specimen. At the end of the test the wrinkle had grown to a length of 65 mm and an amplitude of 16 mm. The amplitude of the wrinkle was taken as the vertical distance from the foot of the wrinkle to the crest and the length was taken as the length between the feet of the wrinkle.

Table 4.1: Experimental Results

	Specimen				
	1	**2**	**3**	**4**	**5**
Global Yield Load (kN)	300	244	300 (23% increase)	208	214 (2.9% increase)
Local Yield Load (kN)	210	142	260 (83% increase)	142	156 (9.8% increase)
Yield Displacement (mm)	10	7.6	7.9	6.2	6
Yield Strain	-0.0025	-0.0018	-0.0018	-0.0019	-0.0019
Ultimate Load (kN)	412	350	408 (16.5% increase)	328	356 (8.5% increase)
Ultimate Displacement (mm)	62.3	22.5	50 (122% increase)	16.7	26 (55.7% increase)
Strain at Ultimate Load (kN)	-0.0217	-0.0098	-0.0192 (96% increase)	-0.0046	-
Wrinkle Load (kN)	407	347	408 (17.6% increase)	313	-
Wrinkle Displacement (mm)	56	17.5	50 (186% increase)	12.5	-
Wrinkle Strain	-0.0271	-0.0145	-0.0192 (32.4% increase)	-0.0124	-

Strain Behaviour

It should be noted that the defect was not developed in the middle of the specimen; hence, the strain behaviour is not symmetric. The strain behaviour discussed in this section refers to the strain values obtained from the strain gage that was closest to the crest of the wrinkle, strain gage 5 (S5 on Figure 4.1).

As shown in Figure 4.4, Specimen 1 shows elastic behaviour until a load of approximately 300 kN, which corresponds to -0.334% strain at the wrinkle crest. After yielding, the compressive strain continues to increase, at a decreasing rate until reaching an ultimate load of 413 kN, corresponding to -2.177% strain. At this point it can be seen that the strain begins to reverse, as a result of the initiation of the wrinkle which creates tension at the crest. After reaching 413 kN, both the compressive strain and the load begin to decrease.

The reduction in compressive strain is a result of the growing wrinkle. As the wrinkle continues to grow the area around the wrinkle expands, thereby decreasing the accumulated compressive strain. The expansion of the wrinkle also reduces the load-carrying capacity of the pipe. When displacement is increased, the wrinkle acts similar to a plastic hinge and allows the pipe to easily bend around the wrinkle rather than staying rigid in order to resist the load. This behaviour can also be seen in Figure 4.3, where the load decreases after 413 kN, when the wrinkle is formed.

It can be found from Figure 4.4 that the strain reversal occurs at the ultimate load of the pipe. Since the strain reversal occurs at the onset of the wrinkle, it can be concluded that the initiation of the wrinkle process indicates not only the local buckling at that section,

but also global buckling of the whole pipe specimen. A picture of the specimen at the end of the test can be seen on Figure 4.15.

4.2 Test 2

Specimen 2 was used to observe the behaviour of a pipe with corrosion of 20% of the wall thickness when subject to bending. The corrosion in the specimen was simulated by machining a 1.2 mm deep corrosion patch, measuring 75 mm by 75 mm, at the center of the pipe (Figure 3.1). Load was applied until a wrinkle formed on the pipe.

As can be observed from Figure 4.5, the specimen shows elastic behaviour similar to that of the uncorroded pipe until reaching the yield load. However, specimen 2 reaches a yield load faster than the uncorroded specimen at 275 kN, 91.6% of the yield strength of specimen 1 (control specimen).

After yielding, specimen 2 continued to carry increased load, showing strain hardening behaviour until reaching an ultimate load of 356 kN, at a displacement of 23.6 mm. It is apparent that the 1.2 mm corrosion patch on specimen 2 reduced the ultimate load of the pipe by 62 kN, or 15% of the strength of the control specimen. It can also be found that the ultimate load was reached at a considerably lower displacement than the control specimen. The displacement needed to reach the ultimate load has been reduced by 39.8 mm, or 64% of the displacement needed for the control specimen to reach the ultimate load.

After reaching an ultimate load of 356 kN, the load decreased while the displacement increased. The loading process continued until a displacement of 63 mm, at which point the wrinkle had grown to a required size.

Strain Behaviour

The strain values that are used in the discussion of strain behaviour of the corroded specimens, specimen 2 – specimen 5, are obtained from the strain gage that is located at the middle of the corrosion patch. Since the wrinkle occurs at the center of the corrosion patch in all four corroded specimens, these strain gages are located at the crest of the wrinkle. The position of the strain gages used in the discussion of strain behaviour of the corroded specimens with respect to the wrinkle and the simulated corrosion patch is indicated as S5 in Figure 4.2.

Figure 4.6 shows the local strain behaviour at the middle of the pipe where the wrinkle defect occurred. While the load-deformation curve shown in Figure 4.5 implies that the pipe shows inelastic behaviour at a load of 275 kN, the strain behaviour in Figure 4.6 shows that the initiation of inelastic behaviour in the pipe starts at a load of approximately 142 kN. This difference is due to the fact that the load-deformation curve shows the global behaviour of the pipe, whereas the strain-load curve in Figure 4.6 only shows the localized strain in one small section of the pipe.

After yielding, the compressive strain at the middle of the pipe continues to increase with the load. When the middle of the corrosion patch reached a strain of -1.45%, it can be observed that the strain begins to reverse, indicating the initiation of the wrinkle. The loss of 20% of the wall thickness has caused the wrinkle defect to form at only 53% of the strain of the uncorroded pipe. This strain gage failed at a displacement of approximately 45 mm. A picture of specimen 2 at the end of the test can be seen on Figure 4.16.

4.3 Test 3

Similar to specimen 2, specimen 3 also had a machined corrosion defect measuring 75 mm by 75 mm, with a depth of 1.2 mm. However, as the purpose of specimen 3 was to analyze the effectiveness of basalt FRP composites on corroded pipe sections, a ten-layered BFRP composite was applied around the corrosion patch. Load was applied in the same manner as the previous tests until the BFRP composite failed.

The specimen did not show a change in stiffness as compared to specimen 2 when load was applied in the elastic range. The reason the stiffness did not noticeably increase may be due to the fact that the basalt fabrics have a relatively low modulus of elasticity as compared to steel. Specimen 3 showed global yielding behaviour at a load of 300 kN, matching the yield strength of the uncorroded specimen.

After yielding, the repaired specimen continued to carry higher load until reaching an ultimate load of 408 kN. The BFRP, applied in the longitudinal direction, helped the corroded pipe reach 99% of the ultimate strength of the uncorroded pipe (412 kN), strengthening the corroded pipe by 16.5%. The load drops observed in Figure 4.7 are caused by cracks in the FRP.

After yielding, the repaired and the uncorroded specimens show similar global behaviour until a load of 350 kN at 14 mm. After this point specimen 3 is able to take more load than the control specimen at a given displacement. This behaviour continues until specimen 3 reaches its ultimate load at 408 kN, reached at a displacement of 50 mm. The composite repair allows the deformation of the corroded pipe to more than double before reaching the ultimate load as compared to the corroded, unrepaired pipe specimen

(specimen 2). After reaching 50 mm displacement, the load-carrying ability of the repaired pipe begins to diminish, while the carrying capacity of the control pipe continues to increase beyond 50 mm due to strain hardening, until it reaches its ultimate load of 412.7 mm at a displacement of 62.3 mm.

The wrinkle formed in the repaired specimen at approximately the same load as the control specimen, 408 kN, however this happens sooner than in the control specimen at only 89% of the displacement. The loading continued until the pipe reached a deformation of approximately 94 mm, at which point the test was stopped since enough data had been obtained to compare this specimen to the control specimen (specimen 1). At the end of the test it was noted that the BFRP did not rupture; instead two longitudinal cracks had formed on the composite (Figure 4.17).

Strain Behaviour

A strain gage attached at the center of the corrosion patch shows the local strain behaviour of the steel pipe at the critical location where the wrinkle formed. The global yielding behaviour of the repaired pipe in the elastic region is very similar to the unrepaired one. As shown in Figure 4.7, the pipe yields at a load of 300 kN and a displacement of 9 mm, which is just slightly higher than specimen 2. Figure 4.8 shows that the local yielding of the mid-corrosion patch takes place at a strain of -0.18%, similar to specimen 2, however the load required to achieve this is 260 kN, an increase from 142 kN in specimen 2. This means that the load required for the weakest part of the pipe specimen to yield has been increased by 83% by the BFRP composite.

Figure 4.8 shows that the reversal of strain in this specimen occurs at a strain of -1.9%. The strain needed to initiate the wrinkle had increased by 33% from the corroded pipe, but is still only 70% of the original pipe. After the initiation of the wrinkle, a reversal of the strain can be seen at the pipe mid-section. However, rather than the load increasing with the decreasing strain as seen in the two previous specimen, the load begins to decrease. This indicates that the wrinkle occurs at the ultimate load and not earlier.

The strain gage failed at a displacement of 64.7 mm. A picture of specimen 3 at the end of the test can be seen on Figure 4.17.

4.4 Test 4

Similar to test 2, the objective of test 4 was to analyze the effect of corrosion on the bending of line pipes. To this end, the pipes were machined with 75 mm by 75 mm defects measuring 40% of their wall depth (2.4 mm). Load was applied on the pipe until a displacement of 55 mm, at which point, the pipe had buckled with a wrinkle defect.

The load-deformation behaviour of specimen 4 is shown in Figure 4.9. There is no noticeable difference in the stiffness of specimen 4 when compared to the control specimen, or specimen 2, with 20% corrosion. However, specimen 4 yields faster than the control specimen, at only 7.85 mm. Consequently, the yield load has been decreased by 17%, dropping from 300 kN to 250 kN.

After yielding, the specimen continues to carry more load until an ultimate strength of approximately 328.7 kN. It should be noted that the ultimate strength of specimen 4, with 40% corrosion, is only 79% of the uncorroded specimen. Also the ultimate load is

reached 3.7 times faster than the control specimen, at a displacement of only 16.7 mm. It is apparent that the corrosion patch, measuring 40% of the wall thickness in depth, has caused the pipe specimen to reach a lower ultimate load at a much lower displacement than the uncorroded specimen and specimen 2.

After reaching its ultimate load, the amount of load carried by the pipe decreases while the displacement increases. The test is continued until the pipe reaches a displacement of 55 mm, at which point a noticeably large wrinkle had grown at the middle of the corroded area.

Strain Behaviour

A strain gage placed at the middle of the corroded area captures the local strain behaviour in the corrosion patch up to the ultimate load, as shown in Figure 4.10. As discussed in section 4.2.1, the yield load shown in the strain-load curve and the load-displacement curve differ since the strain gage capture only the local behaviour while the load-displacement curve shows the global behaviour of the pipe. As shown in Figure 4.10, the corroded area yield at a load of approximately 142 kN, corresponding to a strain of -0.19%. The corroded area with corrosion of 40% of the wall thickness has a yield load comparable to the specimen with corrosion of 20% of the wall thickness. However, the corrosion patch of specimen 4 reaches its yield at only 56.8% of the load that is required by the uncorroded pipe to yield.

After yielding, the corrosion patch shows strain hardening behaviour by taking more load at a decreasing rate. When the center of the specimen reaches a strain of -1.25%, it can be seen that the strain begins to reverse, indicating the initiation of the wrinkle. Due to the

effect of corrosion, the strain needed for the initiation of the wrinkle has been reduced by more than half of that of the control specimen, and the displacement has been reduced by a factor of 4.5.

The strain gage failed at the ultimate load, at a displacement of approximately 16.7 mm. A picture of the specimen at the end of the test can be seen on Figure 4.18.

4.5 Test 5

Specimen 5 was used to analyze the effect of BFRP wrap on pipes with a corrosion depth of 40% of the wall thickness. Therefore, the pipe was machined with a defect matching that of specimen 4, having a depth of 2.4 mm, and wrapped with 20 layered BFRP composite with the fibres oriented in the longitudinal direction. Load was applied until the BFRP composite ruptured.

When comparing the load deformation behaviour of the specimens (Figure 4.11), it can be seen that specimen 5 is slightly stiffer than specimen 4. The stiffness is added by the 20 layers of BFRP wrap attached around corrosion patch which helps the pipe resist bending. The specimen shows yielding behaviour at a load of 214 kN and a displacement of 6mm. It can be seen that the yield load has increased by only 3%, meaning that the FRP has not had a significant effect on the yield load.

As load was increased, a loud cracking sound was heard at a load of 240 kN. It can be seen on Figure 4.11 that the specimen deflects about 1 mm without taking much load; this indicates that a crack has been initiated in the FRP composite. It was noted after the test that this crack was opened further and eventually the crack propagates through all the layers leading to the fracture of the FRP at the top of the pipe (Figure 4.19).

The specimen begins carrying load again at a noticeably reduced stiffness at 7.4 mm. The behaviour of the specimen is similar to the unrepaired pipe until a displacement of approximately 11 mm. After this point, specimen 5 is shown to carry more load than the unrepaired specimen 4 until it reaches its ultimate load of 356 kN at 26 mm. After the pipe reaches a deflection of 26 mm, the crack propagates through all the layers and fully opens up, causing the load to drop by 5% to 337 kN. However, it is apparent that the composite is still contributing to the load carrying capacity since Figure 4.11 shows that the load carried by specimen 5 is higher than specimen 4 after the crack.

It is observed that the cause of the failure of the composite is due to the cross-section ovalization that occurs during bending. As the cross-section deforms, the composite is subjected to tension in the transverse direction of the fibres. Since there is no reinforcement in the transverse direction, the composite will be pulled apart. Through this experiment, it is observed that fibres are necessary in the circumferential direction for the composite to be effective in restoring the load-carrying capacity of a corroded pipe.

It is important to note that the crack in the FRP was parallel to direction of the fibres. Since the basalt fibre used in this project is uniaxial, a crack occurring parallel to the fibre direction means that the strength of the composite is not properly utilised.

Strain Behaviour

The strain gage placed under the FRP, at the middle of the corrosion patch, failed at a strain of -0.019. Therefore, no usable data regarding the initiation of the wrinkle could be obtained for this test. A picture of the specimen at the end of the test can be seen on Figure 4.19.

4.6 Analytical Validation

In order to validate the experimental results, a theoretical equation which relates a section's stress to its moment was used (Equation 4.1). A diagram of the cross section can be seen on Figure 4.13.

$$\sigma_x = \frac{M_z y}{I_z} \tag{4.1}$$

$\sigma_x = bending\ stress$

$M_z = moment\ about\ the\ neutral\ axiz$

$y = perpendicular\ distance\ from\ the\ neutral\ axis\ to\ the\ most\ extreme\ fiber$

$I_z =$ Second moment of area about the neutral axis

This equation is only valid when the stress of the pipe section is in the elastic range. Since the maximum bending stress occurs at the top and bottom of the pipe section, this equation can be used to determine the moment of the pipe when the most extreme fibre of the pipe, the part furthest away from the neutral axis, yields. It was decided to validate the experimental results by comparing the bending moment of the pipe at the onset of yielding behaviour as calculated by Equation 4.1 with the yield strength obtained from the material tests (Figure 4.20).

Based on the location of the supports and loading points, the bending moment can be calculated as a function of the load to be

$$Moment = 325.5 \times Load\ (N \cdot mm) \tag{4.2}$$

where the load is measured in units of N. Since the load at yielding is known for the experimental tests, Equation 4.2 was used to calculate the moment at yielding. Equation 4.1 was used to compute an analytical result for the bending moment at yielding.

The yield stress of the pipe material, as calculated using the uniaxial coupon specimens, is 390 MPa (Figure 4.20). However, due to the internal pressure in the pipe, the stresses formed in the pipe can no longer be considered as uniaxial. The internal pressure acts as a hoop stress on the pipe walls. The hoop stress caused by the internal pressure can be calculated using Barlow's formula:

$$\sigma_h = \frac{PD}{2t} \tag{4.3}$$

$\sigma_h = hoop\ stress$

$P = internal\ pressure$

$D = inside\ diameter$

$t = wall\ thickness$

Since the pipe was subjected to an internal pressure loading of $0.2P_y$ (5.86 MPa), the resulting hoop stress was found to be 106.9 MPa. The internal pressure was kept unchanged during the test.

In the case of biaxial loading, the von Mises yield criterion can be used to predict the resulting yield pressure. The yielding of ductile materials is governed by the maximum shear stress of the material. Since the von Mises yield criterion is based on the maximum distortion strain energy, it is a very good model for predicting the yield surface of ductile metals.

The von Mises yield criterion provides an elliptical yield surface based on the yield stress obtained from a uniaxial tensile test. Using the appropriate load combinations, it can be determined whether or not the material has yielded. Yielding occurs when the von Mises stress reaches the uniaxial yield stress. The reduced von Mises equation is defined as:

$$\sigma_v = \sqrt{\frac{(\sigma_a - \sigma_h)^2 + (\sigma_a)^2 + (\sigma_h)^2}{2}} \tag{4.4}$$

In the above equation, σ_v is set as the yield stress, σ_a is set as the axial stress and σ_h is set as the hoop stress. A graphical representation is presented in Figure 4.14. When solved using the previously determined values, Equation 4.4 will return the axial stress needed to cause the pipe to yield as 325.4 MPa in compression or 432 MPa in tension. This calculation, as well as Figure 4.14, demonstrates that the pipe specimens subjected to an internal pressure of 0.2 p_y, will yield in compression and not tension when bending. As such, when using Equation 4.1 to calculate the bending moment at yielding, a compressive stress of 325.4 MPa needs to be used as the bending stress.

The second moment of area, I_z, is a geometric property that is used to predict the bending behaviour of beam elements with regard to stress and deflection. For a hollow cylindrical cross section, the second moment of area about the neutral axis is calculated as:

$$I_z = \pi \left(\frac{d_o^4 - d_i^4}{64} \right) \tag{4.5}$$

Given an outer diameter of 219 mm, and an inner diameter of 207 mm, the resulting second moment of area is 22,787,381.3 mm^4. Using the above calculated values, the

yielding moment for the experimental results, as well as an analytical value can be determined.

Table 4.2: Moment at yield for experimental tests

Equation	Values	Moment
$Moment = 325.5 \times Load$	Load at yielding	68,355 (N·m)
	210,000 N	

Table 4.3: Theoretical moment at yield

Equation	Values			Moment
$\sigma_x = \frac{M_z y}{I_z}$	σ_x	y	I_z	67,717 (N·m)
	325.4 MPa	109.5 mm	2,2787,381.3 mm^4	

$$\% \, Error = \frac{|68355 - 67717|}{68355} = 0.9\% \tag{4.6}$$

As shown in Equation 4.6, the percent error between the experimental and theoretical value is only 0.9%. Since the difference between the two values is negligible, it can be seen that there is good agreement between the experimental and theoretical results. Therefore, it can be concluded that the results from the experimental values are reasonable and valid.

4.7 Summary

Five specimens of 20% and 40% corrosion were tested, with two specimens having been retrofitted with uniaxial BFRP oriented in the longitudinal direction. The aim of the tests is to analyze and document the effectiveness of BFRP in retrofitting corroded pipes subjected to bending.

A few observations can be made by analyzing the data obtained from these experiments:

1. The yield load and ultimate load decrease as the corrosion depth increases.

2. The displacement needed for the pipe to reach its ultimate load decreases significantly for 20% corrosion – a reduction of 63.8% when compared to the control specimen. Relative to the 20% corrosion specimen, the displacement needed to reach the ultimate load for the 40% corrosion specimen decreased by 25%. As shown in Figure 4.9, the corroded specimens are reaching their ultimate load faster, indicating that the effect of strain hardening is diminished in the post yielding stage due to corrosion.

3. The corroded specimens buckle with a wrinkle defect of a much lower strain as compared to the control specimen. The 20% and 40% corroded specimens developed a wrinkle at a strain of -0.0145 mm/mm and -0.0125 mm/mm respectively, as compared to the virgin pipe which did not develop a wrinkle until reaching a strain of -0.027 mm/mm. Similarly, for specimens 2 and 4, the wrinkle occurs at lower displacements, 17.5 mm (31%) and 12.5 mm (22%) respectively, relative to the control specimen.

4. The addition of ten layers of BFRP in specimen 3 greatly delays the wrinkle. The displacement needed for the wrinkle initiation has increased by 185% from specimen 2.

5. The repaired specimen 3 was able to reach an ultimate load of 408 kN, 99% of the uncorroded specimen, at a displacement of 50 mm; which is an increase of 122% from specimen 2.

6. Unlike specimen 3 which only formed cracks, the composite repair of specimen 5 failed by completely rupturing parallel to the fibre direction, meaning the failure occurred in the matrix and the strength of the fibres was not fully utilized. It is evident that the ovalization of the cross-section and the expansion of the wrinkle cause the fibres to be pulled apart before reaching their ultimate tensile or compressive strength in the fibre direction. Therefore, it is necessary to orient the fabric in the circumferential direction in addition to the longitudinal direction.

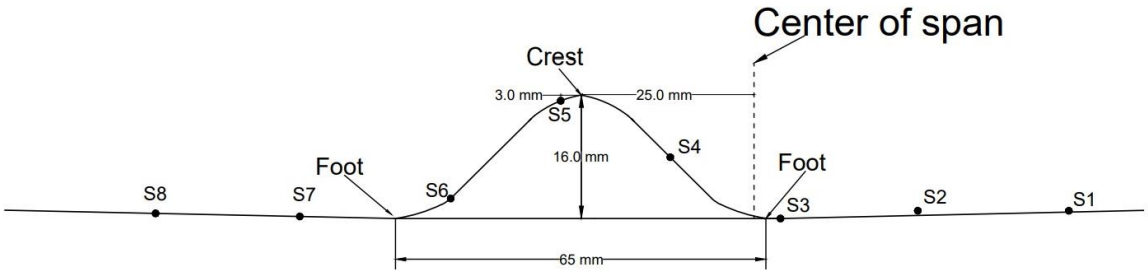

Figure 4.1: Location of strain gages for specimen 1

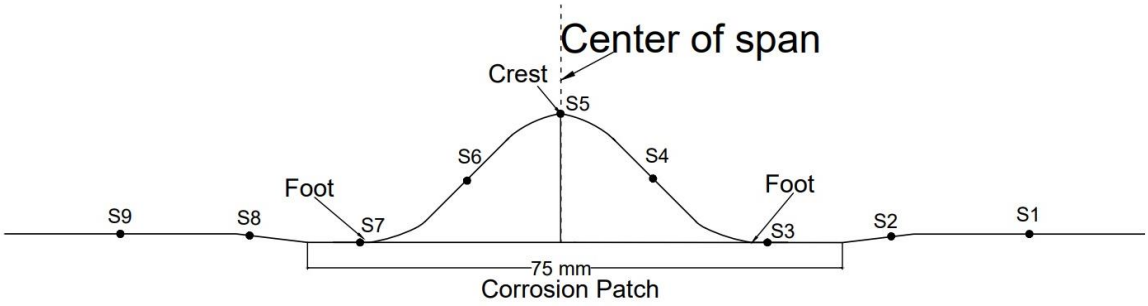

Figure 4.2: Location of strain gages for corroded specimens

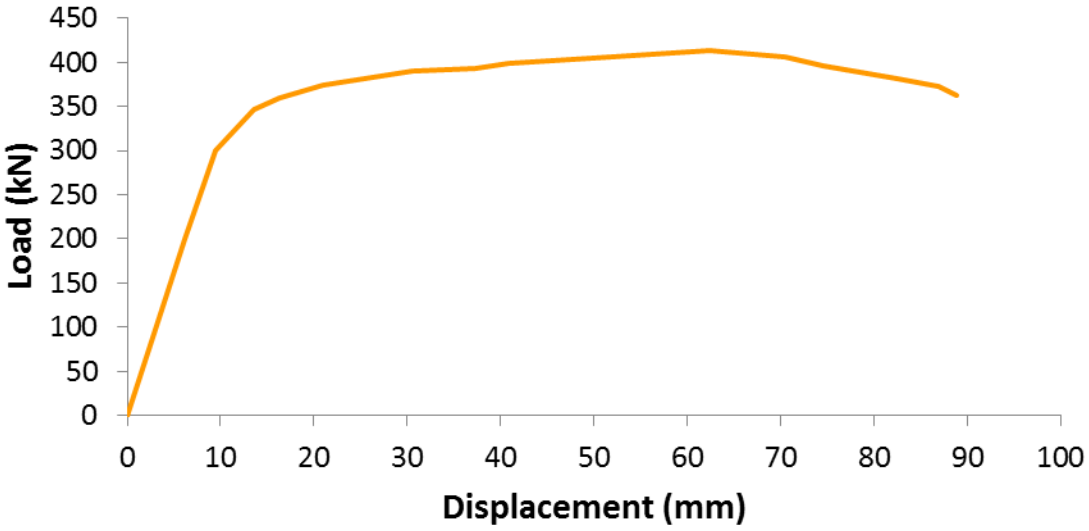

Figure 4.3: Load-displacement curve of Specimen 1

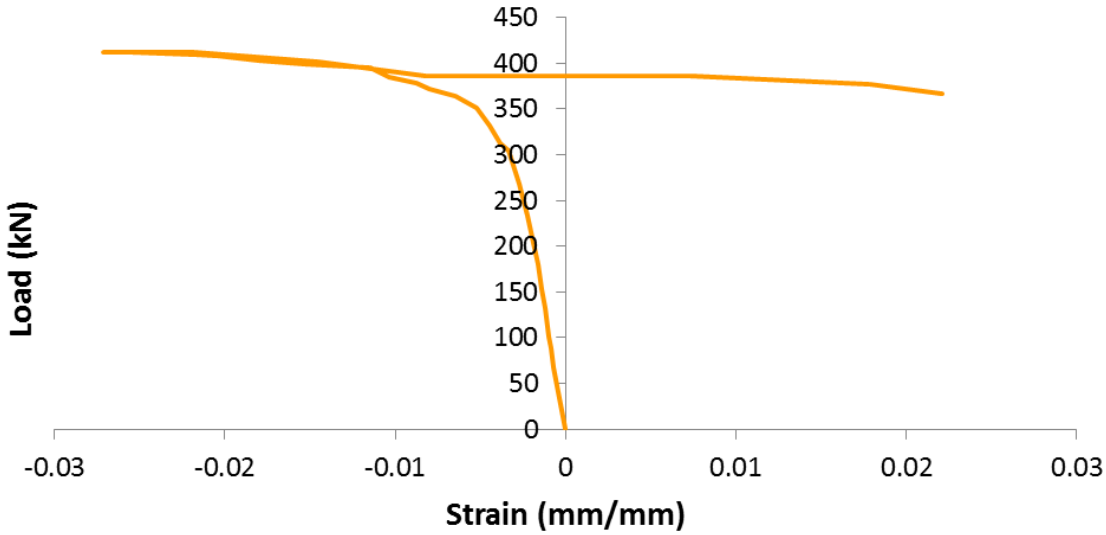

Figure 4.4: Strain behaviour at the wrinkle location of Specimen 1

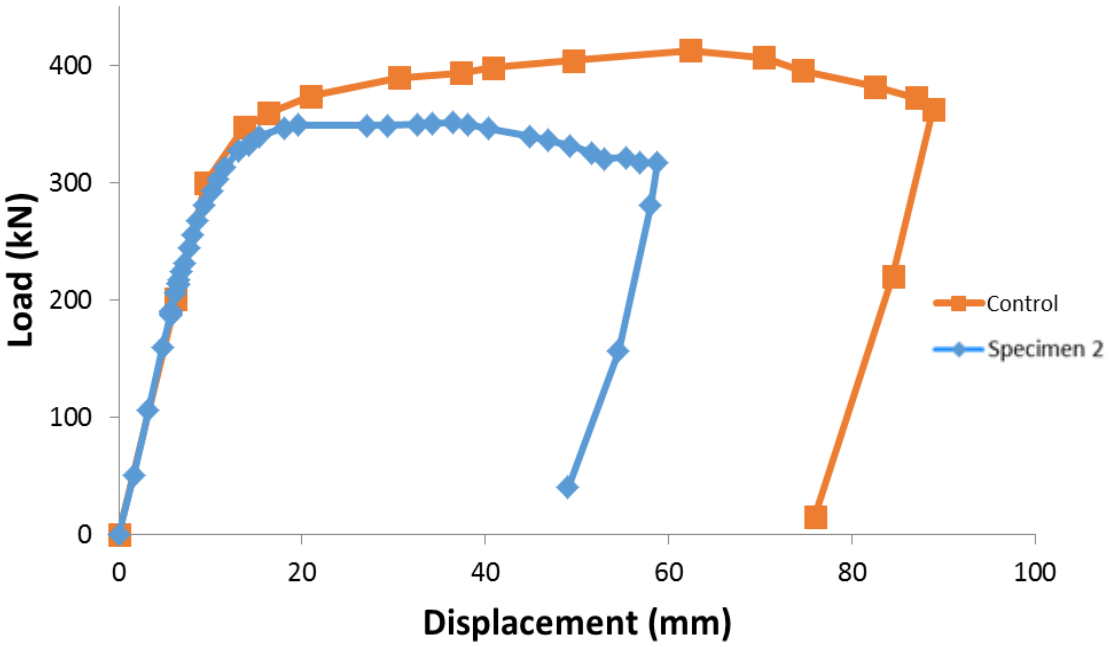

Figure 4.5: Comparison of load-deformation curves for Specimen 1 and Specimen 2

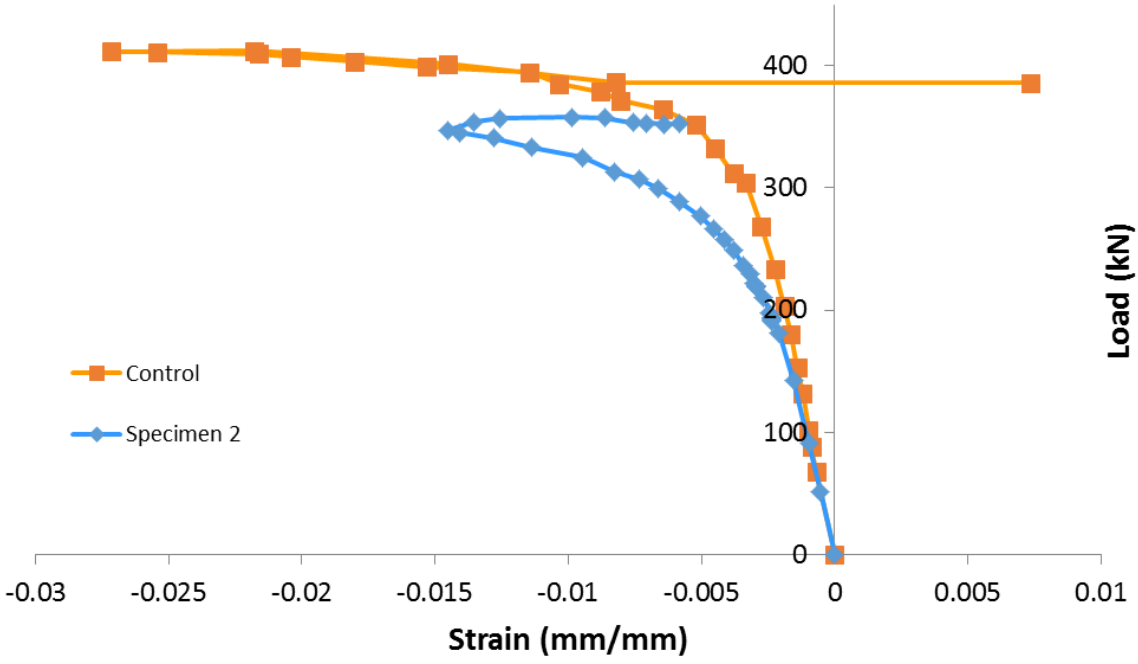

Figure 4.6: Comparison of strain behaviour at the wrinkle location of Specimen 1 and Specimen 2

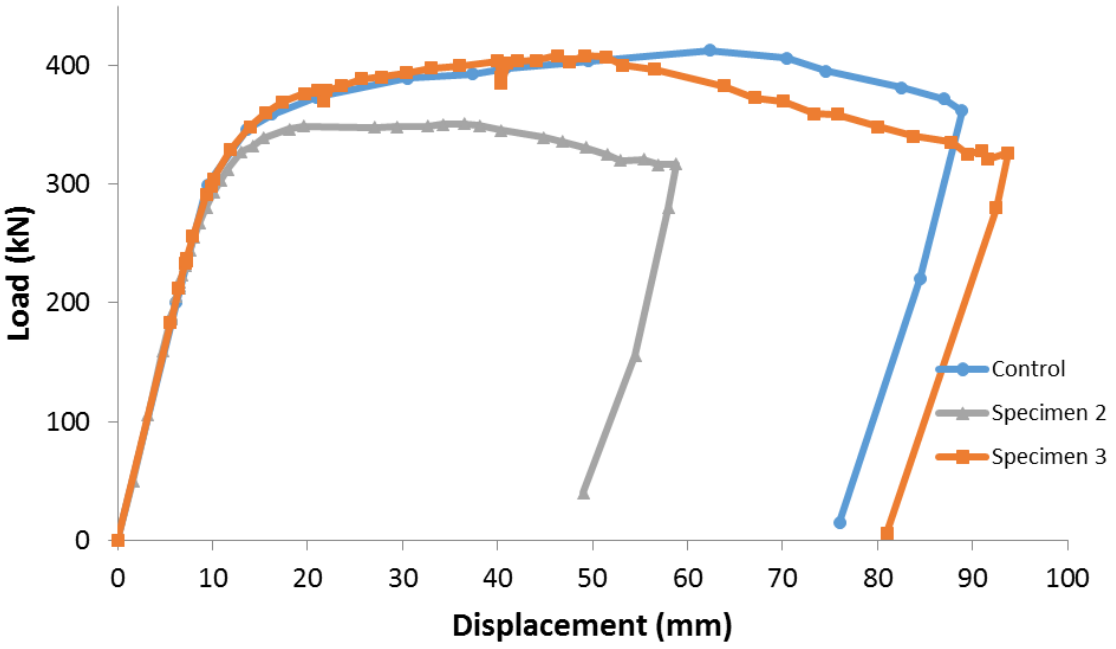

Figure 4.7: Comparison of load-deformation behaviour of Specimen 3 with Specimen 1 and Specimen 2

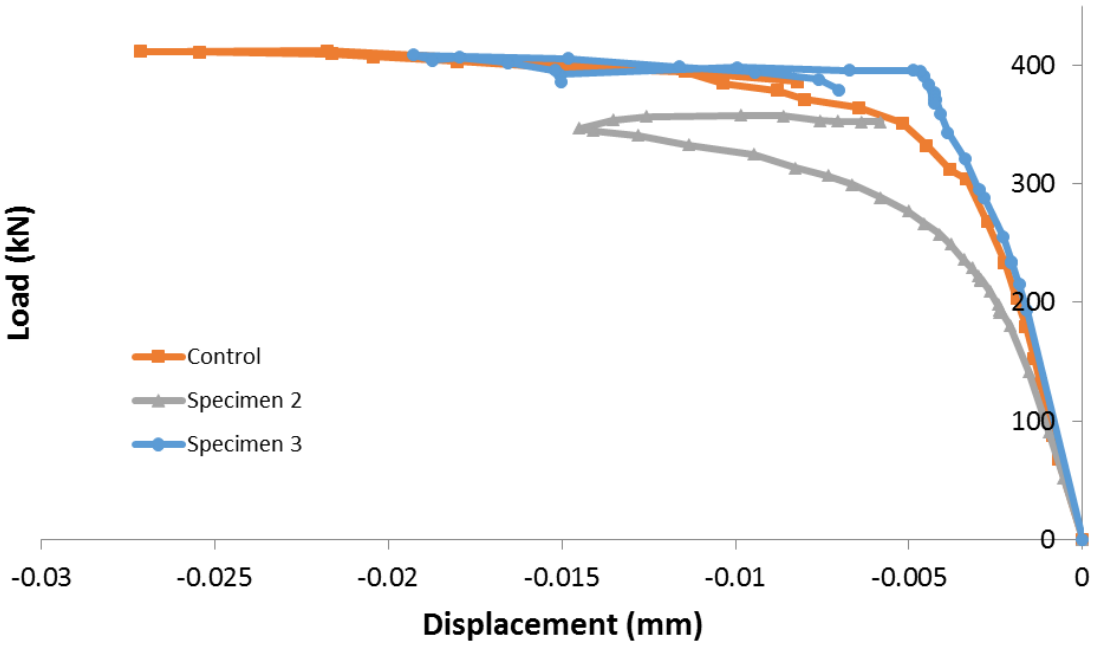

Figure 4.8: Comparison of strain behaviour at the wrinkle location of Specimen 1, Specimen 2 and Specimen 3

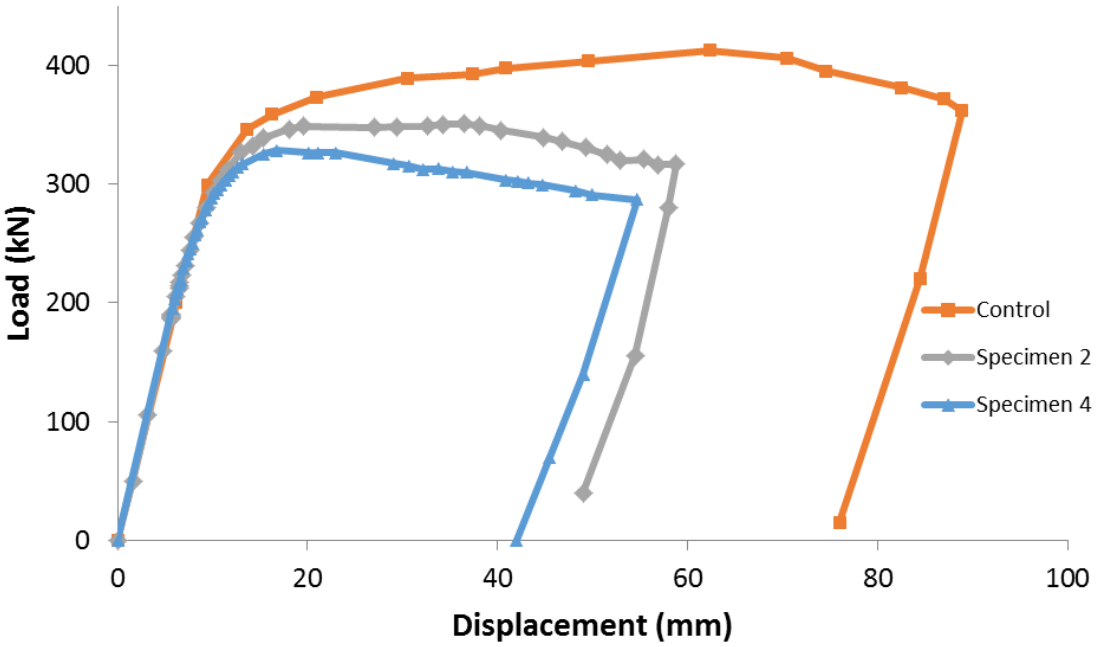

Figure 4.9: Comparison of load-deformation behaviour of Specimen 4 with Specimen 1 and Specimen 2

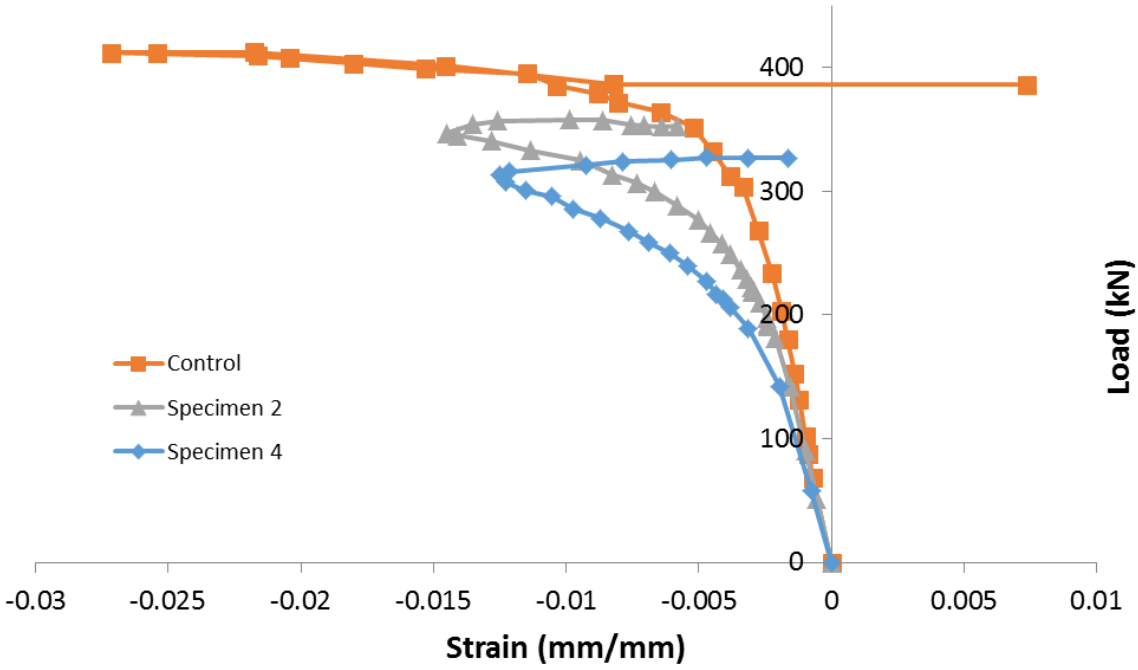

Figure 4.10: Comparison of strain behaviour at the wrinkle location of Specimen 1, Specimen 2 and Specimen 4

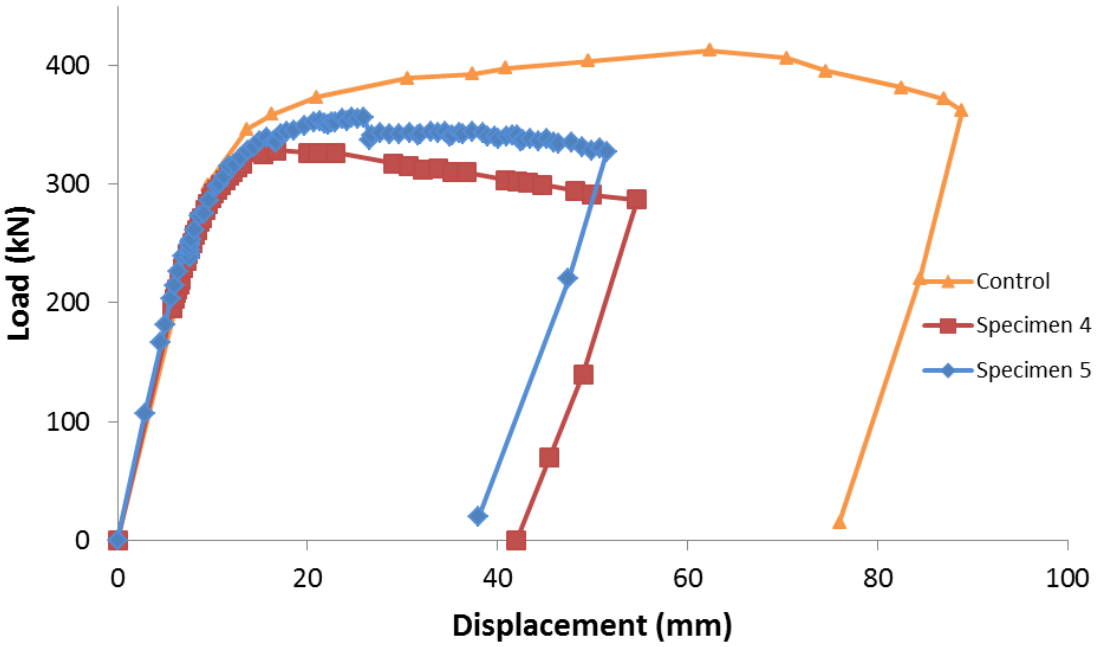

Figure 4.11: Comparison of load-deformation behaviour of Specimen 5 with Specimen 1 and Specimen 4

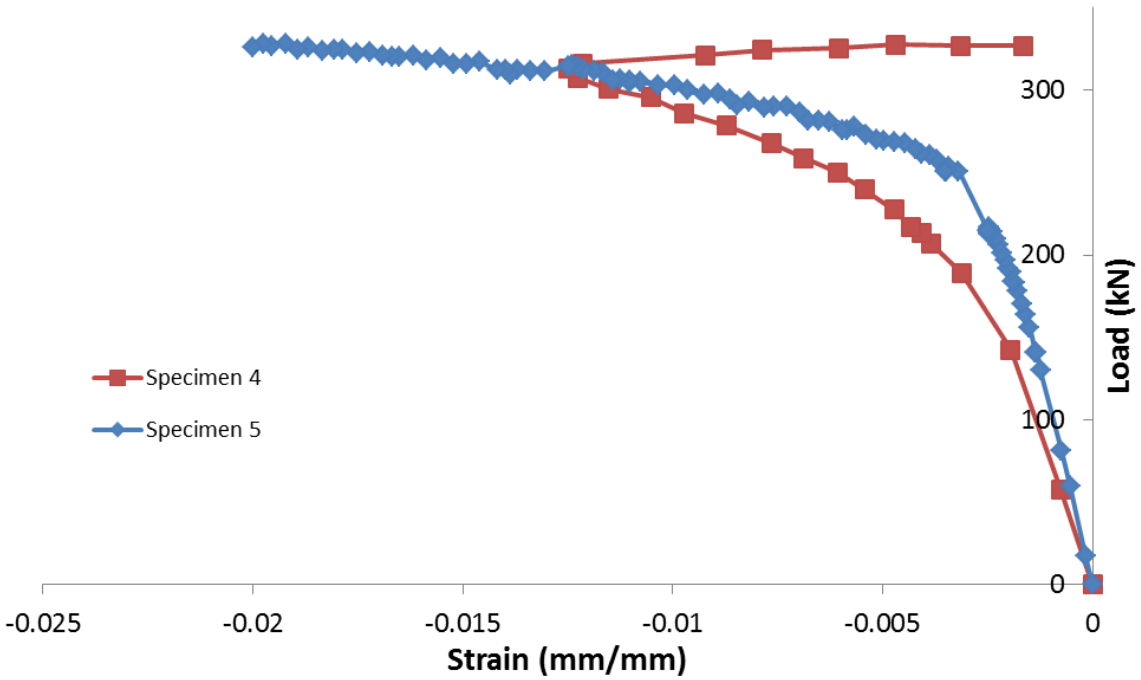

Figure 4.12: Comparison of strain behaviour at the wrinkle location of Specimen 5, Specimen 4

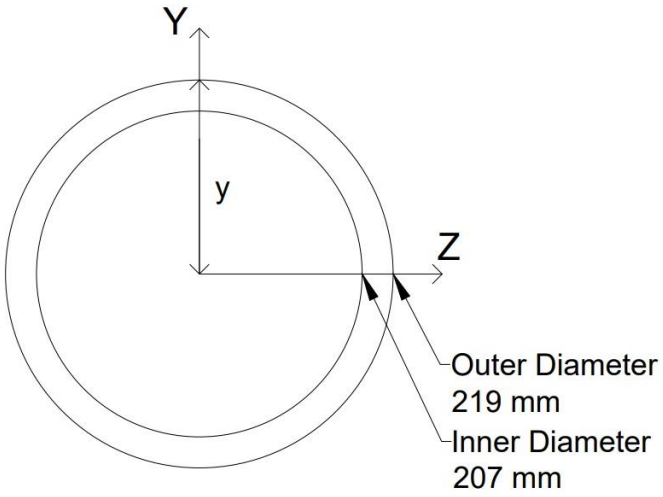

Figure 4.13: Cross-section of the pipe specimen

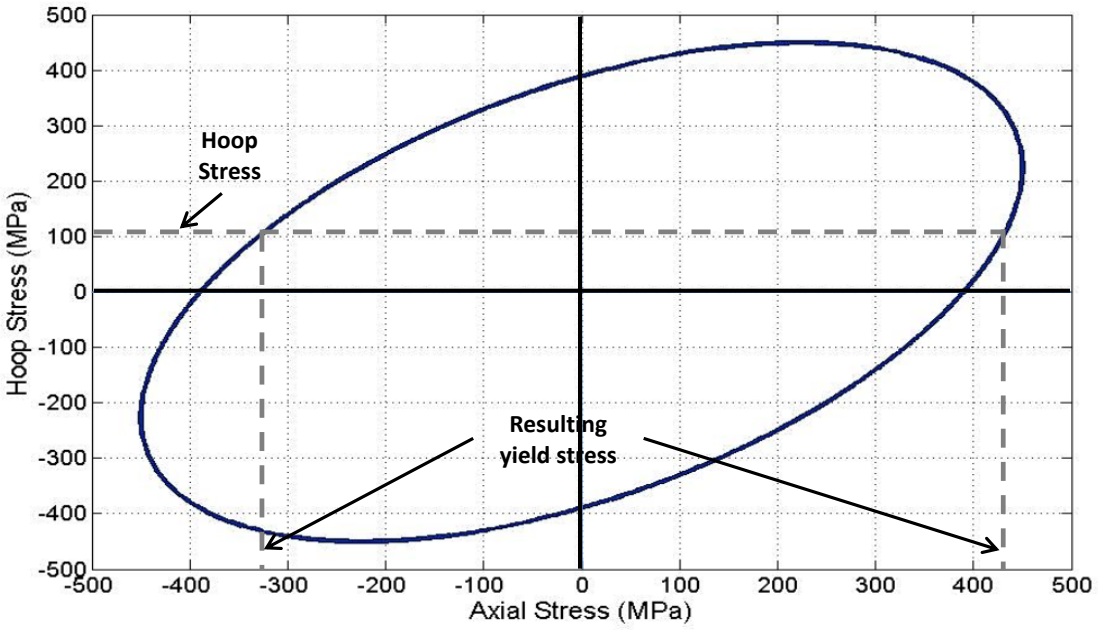

Figure 4.14: Axial stress needed to cause yielding due to the hoop stress according to the von Mises yield criterion

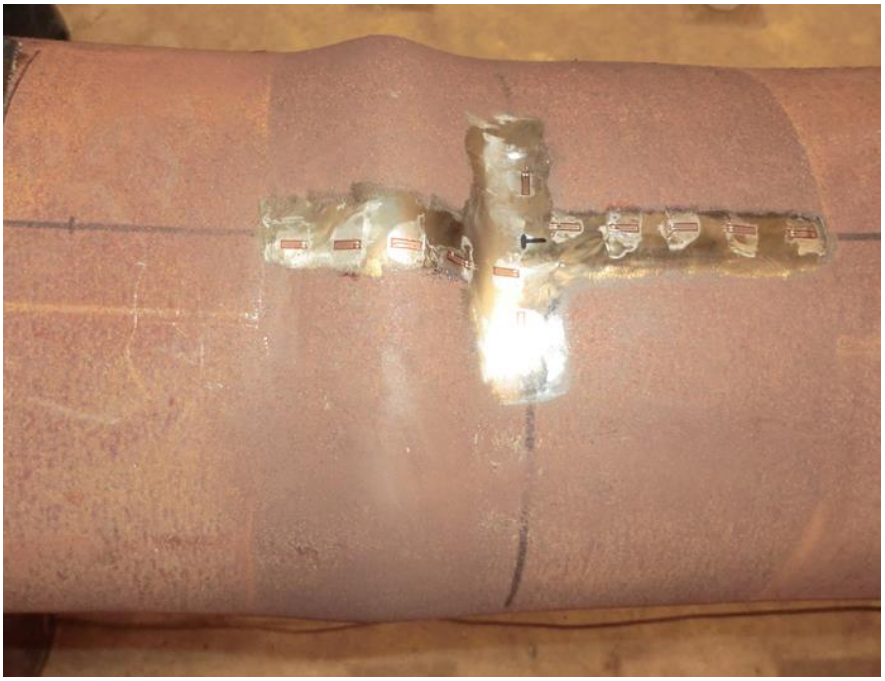

Figure 4.15: Specimen 1 after testing

Figure 4.16: Specimen 2 after testing

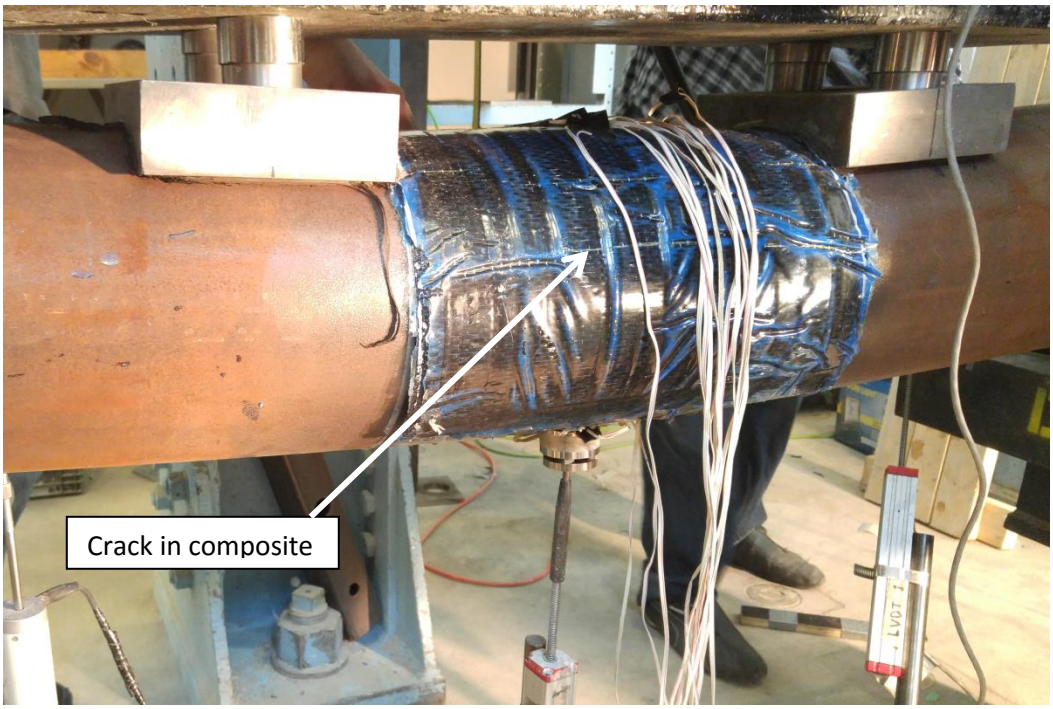

Figure 4.17: Specimen 3 after testing

Figure 4.18: Specimen 4 after testing

Figure 4.19: Specimen 5 after testing

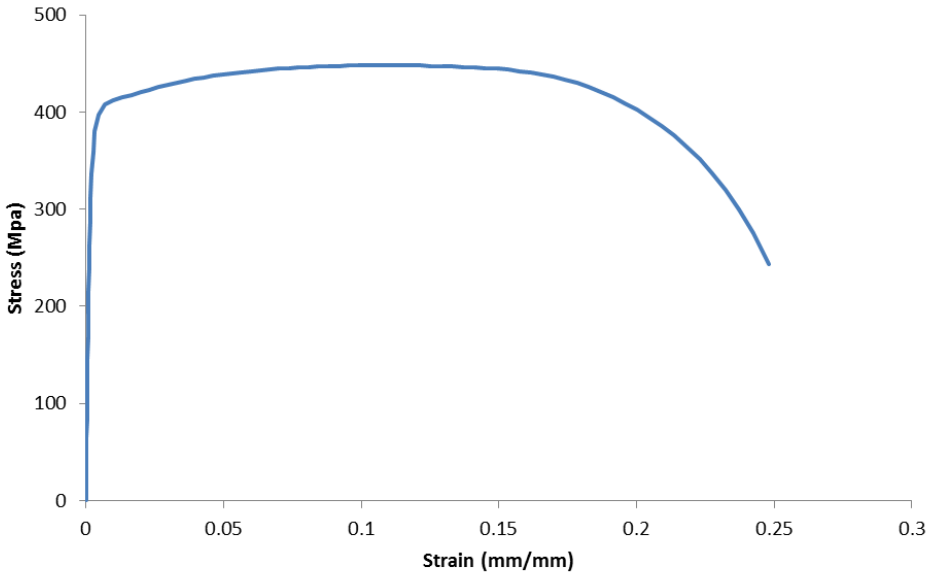

Figure 4.20: Engineering stress-strain curve of steel coupon

Chapter 5 Finite Element Analysis

5.1 General

Due to costly and labour-intensive nature of full-scale experimental tests, it is challenging to conduct full-scale tests for every parameter. In order to predict the effect of varying FRP layers and directions, the use of Finite Element Analysis was implemented. The software suite chosen for this purpose is Abaqus/Standard, which is capable of producing highly accurate analyses of static and low-speed dynamic events.

There are three stages in finite-element analysis: pre-processing, processing, and post-processing. Abaqus is capable of performing all three of these stages. The pre-processing stage consists of modeling the design either using a graphic user interface, or through the use of an input file. In this stage, the user defines the part geometries, material properties, loads and boundary conditions as determined by the design. There are many other compatible CAD software that are capable of completing the pre-processing stage, however because of the user-friendly interface provided by Abaqus, the modeling of the pipe specimen was prepared in the program.

The analysis of the problem takes place in the processing stage. The method of analysis varies between different software. Abaqus formulates finite element equations to define the model submitted by the pre-processor. The number of equations depends on the complexity of the model, and in turn is a factor in determining the amount of time taken to complete the analysis. Abaqus allows the user to divide the analysis procedure into several steps and specify the incrementation scheme for each step. Then at each increment, Abaqus/Standard attempts to implicitly solve a system of equations. For

nonlinear problems, Abaqus/Standard generally uses the iterative Newton's method while the stiffness method is used for linear problems.

Post-processing consists of viewing the results of the analysis, typically by generating a report of the requested output variables or visualizing the results in 2D or 3D space. Abaqus allows the user to plot variables, generate contours of different variables and provides animation of the deformation of the model throughout the analysis in the post-processing stage.

In order to validate the FEA results the five lab tests were modeled in Abaqus. The accuracy of the model in predicting the behaviour of pipes with new parameters would be determined by how well the experimental data of the five specimen match up to the data from the FEA for models of those five specimen. The comparison criteria between the analytical and experimental results will consist of the load, deformation behaviours of the specimen.

5.2 Model

5.2.1 Assembly

Pipe

Thirteen part instances were modeled and assembled to represent the test setup that was used in the experimental part of the project. The thirteen part instances include: the pipe specimen, four supports (two at the bottom and two at the top), end caps at each end, and six collars. The geometry of each part was made as close to the real part as possible.

The Abaqus user manual recommends using shell parts to model structures whose thickness is significantly lower than the other directions. However, the pipe specimen was modeled as a solid part in order to model the corrosion defect. For each corrosion depth studied, a 75 mm x 75 mm section was removed from the outer surface of the pipe at the top. This process creates a sharp 90o cut which was corrected with the fillet tool in order to create a 10 mm taper.

The part instances in the finite element model were assembled to imitate the experimental setup as closely as possible. The bottom supports were placed at a distance of 1810 mm apart, and the top supports were placed 500 mm apart, same as was done in the experimental setup. Coaxial constraints were placed on the pipe and support surfaces when assembling the model so that there are no gaps between the two surfaces. Coaxial constraints were also placed on the six collars, which were positioned on either side of the top supports. The end caps were attached to the pipe ends using tie constraints. Figure 5.1 shows the pipe specimen modeled in Abaqus.

FRP Composite

The FRP composite was modelled as a cylinder composed of continuum shell elements, with an inner diameter of 219 mm – same as the outer diameter of the pipe. The part was assigned composite layup section properties. This allows the user to specify the desired number of layers (plies) to be used in the composite, as well as the desired thickness of each ply as well as the angle of rotation. Therefore, the part was modelled as one monolithic piece, with each individual layer of the fabric defined in the composite layup section properties.

5.2.2 Interaction

Abaqus offers several different ways to define the interaction between parts. The interaction between the pipe surface and the supports and collars were defined as surface-to-surface contact. The stiffer surfaces of the supports and collars were selected as the "master" surface and the less stiff surface of the pipe was selected as the "slave" surface. In order to define the normal behaviour of the surfaces, the Hard Contact option was used. This configuration enforces the contact constraint by allowing an unlimited amount of contact pressure to be transmitted between the surfaces. The tangential behaviour of the surfaces was defined using a friction coefficient of 0.3, which is typical for steels.

The interaction between the FRP composite and the pipe was represented using a tie constraint and surface-to-surface contact. Defining the surface-to-surface contact in addition to the tie constraint is necessary in order to define the normal behaviour between the two parts.

5.2.3 Loads and Boundary Conditions

Once the model was assembled the loads and boundary conditions were placed on the model. The boundary conditions were applied to the top and bottom supports similar to the physical setup. The bottom supports were restrained in translation in all directions and rotation around the y and z–axes. The top supports were allowed to rotate about the x-axis, and translate in the y-direction. By allowing the supports to rotate, the supports are able to conform to the curvature of the pipe. The top supports must be allowed to translate vertically, in order to apply load. Since the loading of the experimental test was displacement-controlled, the load on the top support was applied as a displacement boundary condition.

5.2.4 Material Properties

Pipe

The Abaqus software requires the user to define the material properties of all deformable parts in order to run the simulation. Including many material properties, such as: inelastic behaviour, damage parameters, etc. will allow for a more comprehensive analysis.

Using the data obtained from coupon tests, the elastic and plastic material behaviours of the pipe were defined. Since the pipe material is steel, the elastic behaviour of the pipe was defined as isotropic. The elastic material properties used for the pipe can be seen in Table 5.1

Table 5.1: Elastic material properties of the pipe

E	μ
160 GPa	0.3

The plastic material behaviour is used to define the strain hardening and softening behaviour of the material that occurs after yielding. Abaqus requires the stress and strain inputs to be in terms of the true (Cauchy) stress and logarithmic strain. Since stress-strain data is available from uniaxial coupon tests, the nominal stress and strain were converted to true stress and logarithmic strain using equations 5.1 and 5.2, respectively.

$$\sigma_{true} = \sigma_{nom}(1 + \epsilon_{nom}) \tag{5.1}$$

$$\epsilon_{ln} = ln(1 + \epsilon_{nom}) - \frac{\sigma_{true}}{E} \tag{5.2}$$

Table 5.2 presents the plastic material properties of the pipe. The true stress-strain curve of the steel pipe specimen can be seen on Figure 5.2

Table 5.2: Plastic material properties of the pipe

Stress (MPa)	Plastic strain
390.9368129	0
419.74517	0.010091
433.7718883	0.020994
446.2555694	0.031624
457.0744177	0.042284
466.5259832	0.053059
474.8873066	0.063974
482.3671928	0.074988
489.082972	0.086118
495.2325801	0.097362
500.7734754	0.108744
505.7280122	0.120268
509.7942829	0.131958
515	0.212638

BFRP

In order to assign material properties to the composite layup parts, the user must specify the material orientation in a local coordinate system. The local direction 1 corresponds to the longitudinal direction of the fibre, local direction 2 corresponds to the transverse direction of the fibre and the local direction 3 corresponds to the normal direction of the ply. The BFRP composite was modeled as one homogenous section, and the thicknesses, material properties and the orientations of each layer of fabric was defined within the

program. Figure 5.5 shows the local coordinate system of the FRP section, with local direction 1 oriented in the longitudinal direction of the composite, local direction 2 oriented in the tangential direction of the composite and local direction 3 in the radial direction of the composite. The material properties of the BFRP composite were determined through coupon tests in order to be used in the model. Table 5.3 outlines the elastic material properties used for the composite.

Table 5.3: Elastic material properties of the composite

E1	E2	Nu12	G12	G13	G23
20432	8000	0.35	204.32	204.32	102

5.2.5 Elements

Abaqus has a vast library of elements that can be used to model different types of structures. For the purposes of this project, the following element types were used: C3D8R and C3D20R – 8 and 20-node brick elements, SC8R – 8-node continuum shell elements, and R3D4 – 4-node rigid quadrilateral elements.

Shell elements are used in Abaqus to model structures whose thickness is significantly smaller than the other dimensions. Continuum shells differ from the conventional shells by the way the thickness of the structure is defined. The thickness of structures modelled using conventional shells is defined using section properties; while the thickness of structures modelled using continuum shell elements is defined using the nodal geometry. SC8R elements, used to model the composite section, are 8-node planar elements, meaning the stresses and strains of the element are only measured in the plane that is orthogonal to the thickness of the element.

C3D8R and C3D20R elements are 8-node and 20-node general purpose linear brick elements with reduced integration. The reduced integration helps decrease the artificial stiffening effect that is seen in fully integrated elements. The C3D20R quadratic brick elements were used to model 200 mm of the middle portion of the pipe where the wrinkle is expected to occur. The quadratic elements were used for the mid-section since they have twenty nodes, and are expected to capture the bending behaviour more accurately than the eight node element. The mesh was generated to include two elements through the wall thickness.

5.3 Mesh Convergence Study

A mesh convergence study was conducted for two purposes. Firstly, it is important to determine whether the model is correct and the results converge at finer mesh densities. Secondly, generating meshes with different densities allows the user to choose a mesh density that allows a good balance between accuracy and speed of the solution.

Since the pipe specimen is the main focus of the simulation, only the pipe's mesh was considered in the study. The meshes of the other parts (collars, supports, end caps) were adjusted accordingly to satisfy the contact and constraint requirements of the program. The mesh density was varied as shown in Table 5.4.

Table 5.4: Effect of mesh density on the accuracy and duration of analysis

Element Size	Number of elements	Stress (MPa)	% error	Time to complete (sec)
3x3	7872	524.365	0	8055
5x5	4726	508.184	3.08	6490
10x10	3044	645.347	23.07	5357
15x15	1442	838.039	59.82	2067

Table 5.4 lists the element sizes used in the study, resulting number of elements, the percentage of error exhibited by each element relative to the finest mesh (3x3), and the time taken for the simulation to complete. As shown by Table 5.4, the mesh with 15x15 elements in the middle takes the shortest time to complete; however, it is the most inaccurate mesh. As the element size decreases, the time needed for the analysis to complete increases, but the error decreases.

Figure 5.6 contains a graphical representation of the mesh convergence study. The graph plots the stress vs. the mesh density of each element size. The mesh density, on the x-axis, is represented by the number of elements in the midsection. The stress, on the y-axis, is the Mises stress at the middle of the pipe on the compression side at the end of the loading step.

It can be seen on Figure 5.6 that as the mesh size at the middle is reduced from 5 mm to 3 mm, the stress at the middle of the pipe converges 445 MPa. Therefore, the mesh size at the midsection of the pipe was set to be 3 mm.

5.4 Validation of the model

In order to use the finite element modelling to predict the behaviour changing the composition of the BFRP composite, it must be verified that the simulated model acts similar to the real-world test. Therefore, the load-deformation curves generated by the finite element models were compared to the experimental results (Figures 5.7-5.11).

Figures 5.7, 5.8 and 5.9 compare the load deformation behaviours of the experimental and simulated load deformation curves of the control specimen, 20% corroded specimen, and 40 % corroded specimen, respectively. Figures 5.10 and 5.11 compare the load deformation curves of the simulated and experimental results of the pipes repaired with BFRP wrap. Figure 5.11, which compares the experimental and analytical load-deformation curves of specimen 5, shows a gap in load at a deflection of approximately 25 mm. This is due to the fact that the damage evolution criteria was not specified for the basalt composite; therefore, the FEA model did not simulate the rupture in fabric, and the resulting drop in load carrying capacity. However, it can be seen that overall the results of the FEA simulation are similar to what was seen in the laboratory tests. Therefore, it is assumed that reasonably accurate results can be achieved through the use of this model.

5.5 FEA Models

Since the pipe specimen with corrosion measuring 40% of the wall thickness did not reach the load-carrying capacity of the original pipe after repair, it was decided to model that specimen with varying thicknesses of the BFRP composite. It was seen in specimen 5 that when repairing corrosion of 40% of the wall thickness, the composite ruptured parallel to the fibres. In order to prevent the rupture, a few models were made with the

fibres of the composite oriented in the longitudinal direction as well as the circumferential direction. Table 5.5 presents the parameters that were studied for the FEA simulation. The orientation of the fabrics for model 5 can be seen on Figure 5.5.

Table 5.5: Test matrix for the FEA simulation

Model	Layers in the longitudinal direction	Layers in the circumferential direction
1	0	0
2	20	0
3	40	0
4	60	0
5	10	10
6	15	15
7	20	20
8	30	30

Eight models were created according to the above test matrix. The loading process was simulated using the Abaqus software, replicating the experimental procedure. An analysis of the results obtained from the simulations is presented in the next section.

5.6 Results

This section discusses results of the finite element analysis in terms of the load-deformation response and the ultimate lateral load capacity of the specimens. The effect of increasing layers in the longitudinal direction and adding layers in the circumferential

direction is discussed. Table 5.6 presents the number of layers and the ultimate load achieved by each specimen that was studied.

Table 5.6: Results of the FEA simulation

Model	Layers in the longitudinal direction	Layers in the circumferential direction	Ultimate Load (kN)	Increase in ultimate Load
1	0	0	334	0%
2	20	0	361	8.1%
3	40	0	365	9.3%
4	60	0	374	12.0%
5	10	10	355	6.3%
6	15	15	361	8.1%
7	20	20	363	8.7%
8	30	30	368	10.2%

It can be seen from Table 5.6 that as the layers increase in the longitudinal direction, there is an increase in the ultimate strength. Attaching 20 layers of BFRP composite in the longitudinal direction yields an ultimate strength of 8.1%. However, attaching another 40 layers increases the strength by only 3.9%. This can also be seen in Figure 5.12, which shows the load-deflection curves of models 2, 3 and 4. The increase in load-carrying capacity is marginal.

Figure 5.13 is a visual representation of Table 5.6, which plots the ultimate load and the number of layers. It is apparent that as the number of layers increase, the ultimate strength increases at a decreasing rate. This is similar to the result seen by Elchalakani

(2016). Figure 2.6 shows a plot by Elchalakani, where a pipe with corrosion of 20% of the wall thickness is repaired by two and four layers of carbon FRP. The repair made using four layers of fabric marginally outperforms the repair made using two layers of CFRP.

Figure 5.13 also demonstrates that orienting fibres in the circumferential direction has a negligible effect on the bending capacity of a pipe. A repair made using fibres oriented in both the longitudinal and circumferential directions has a lower ultimate load than a repair that is made using the same number of layers in the horizontal direction. However, placing fibres in the circumferential direction is necessary in a composite repair, in order to carry the hoop stress caused by the internal pressure.

Analysis of additional corrosion depths were not conducted since it was obvious that the pipe specimen with 40% corrosion of the wall thickness could not be repaired by using as much as 60 layers of BFRP to attain the performance of the virgin pipe.

5.7 Summary

As described in this chapter an FEA study was conducted using commercial Abaqus software in order to observe the effects of attaching additional layers of BFRP fabrics in the longitudinal direction, as well as adding BFRP fabrics in both the longitudinal and circumferential directions. By analyzing the results obtained from this study, the following conclusions can be drawn:

- Attaching FRP composites with fibres oriented in the longitudinal direction will improve the bending behaviour of the pipe. However, after a certain number of

layers, the increase in improvement will be marginal, and the cost will far outweigh the benefit.

- The ultimate load achieved by using fabrics in the longitudinal and circumferential direction is lower than that achieved by orienting the same number of fabrics in the longitudinal direction.

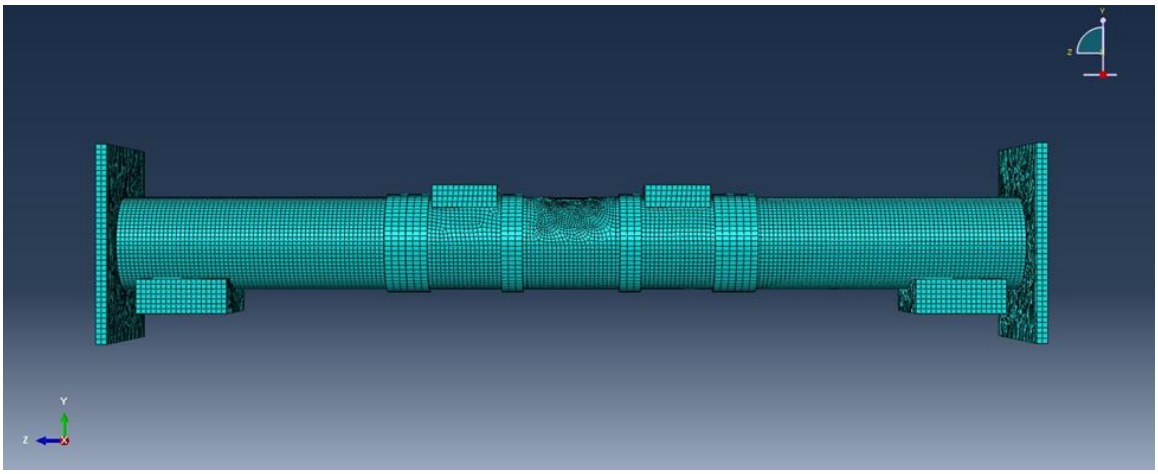

Figure 5.1: Pipe specimen modeled using Abaqus software

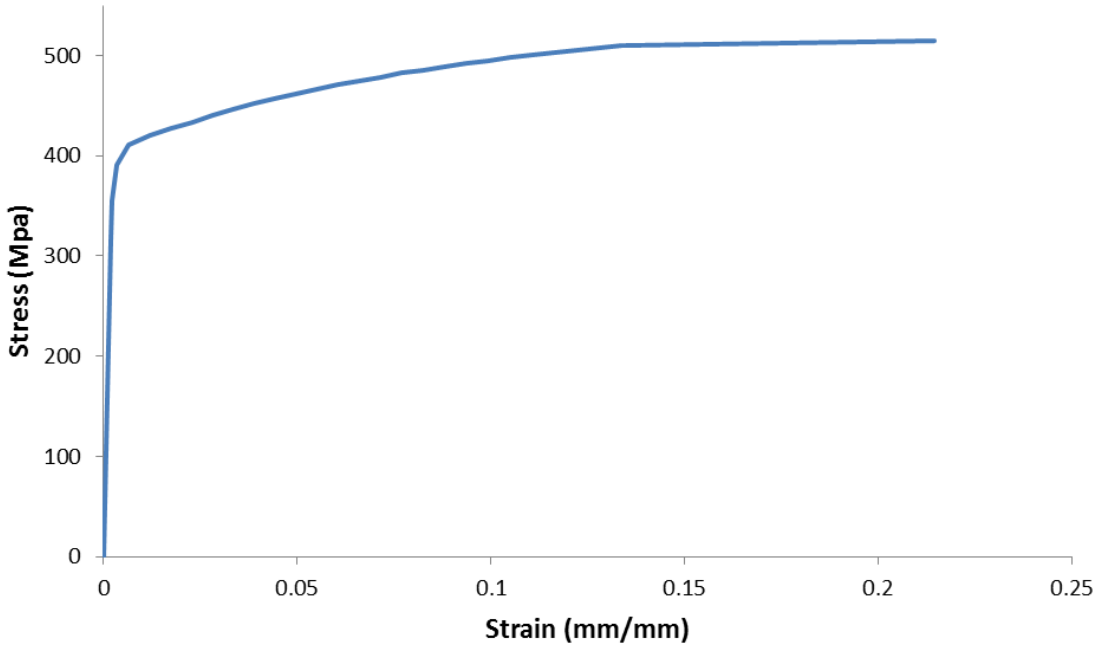

Figure 5.2: True stress-strain curve of the steel pipe

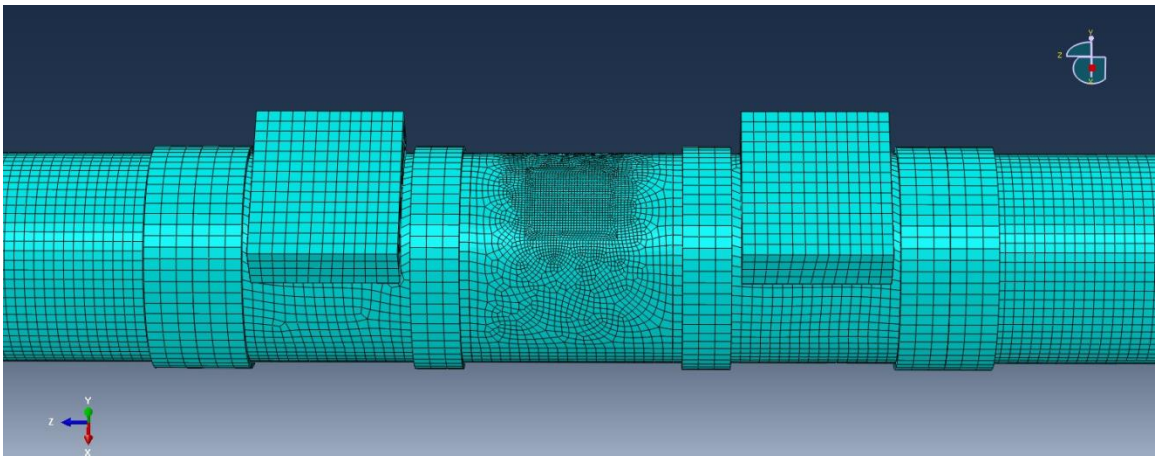

Figure 5.3: Higher mesh density at the middle

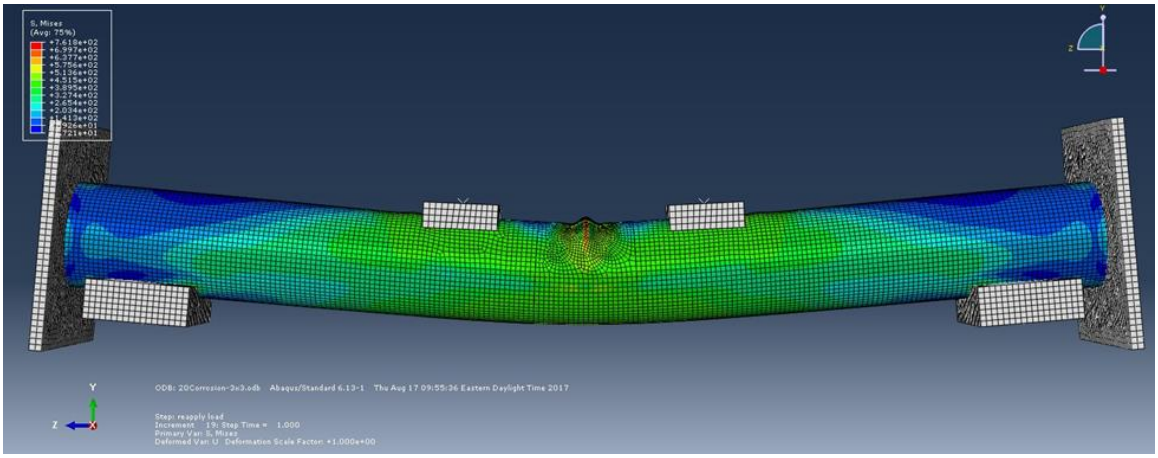

Figure 5.4: Pipe specimen with wrinkle defect after bending

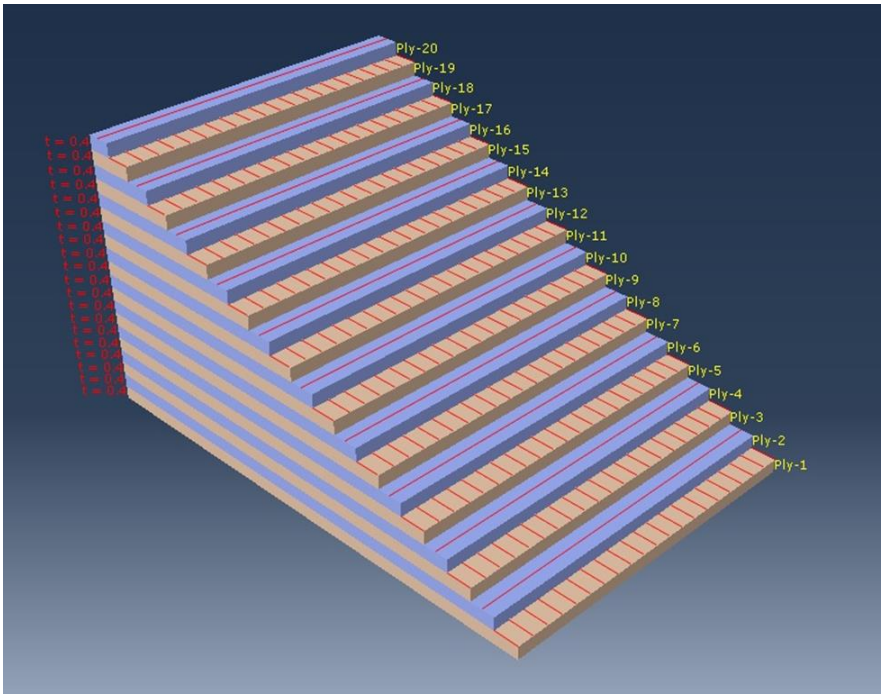

Figure 5.5: Orientation of the BFRP fabric with ten layers oriented in the longitudinal direction and ten layers oriented in the circumferential direction

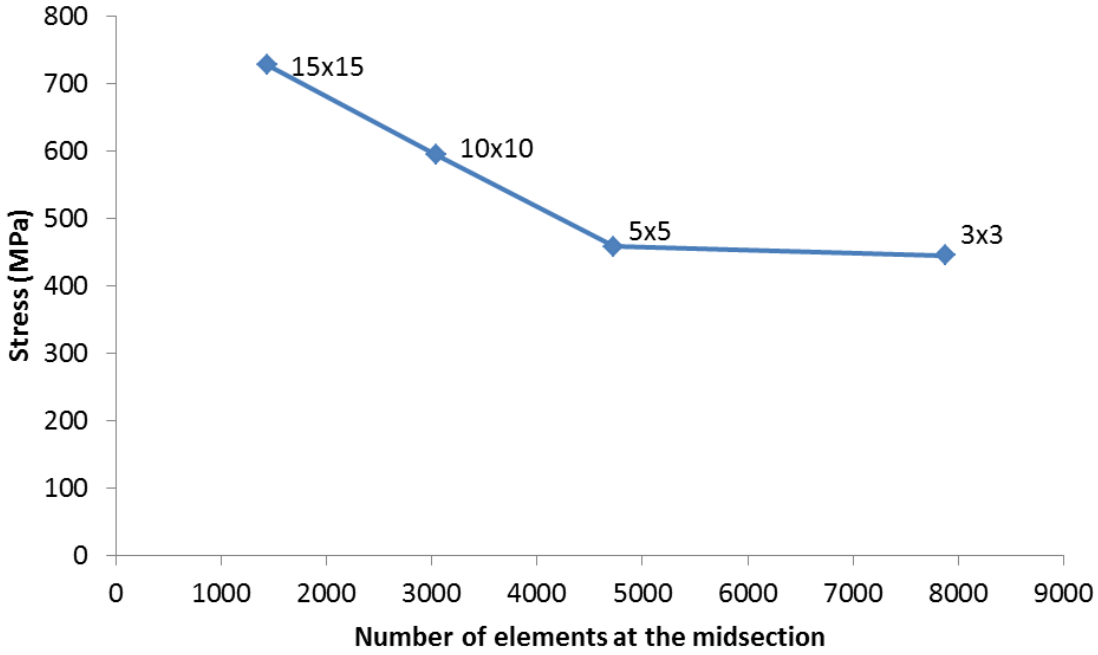

Figure 5.6: Plot of stress vs. mesh density

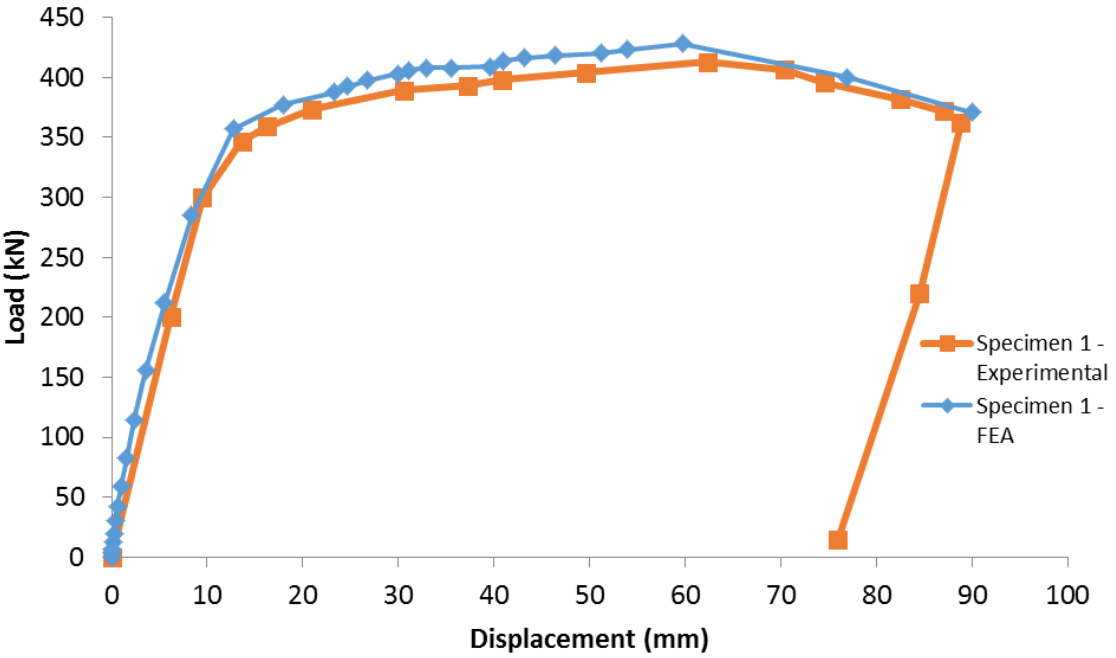

Figure 5.7: Comparison of load-displacement curves of Specimen 1 - experimental and simulated

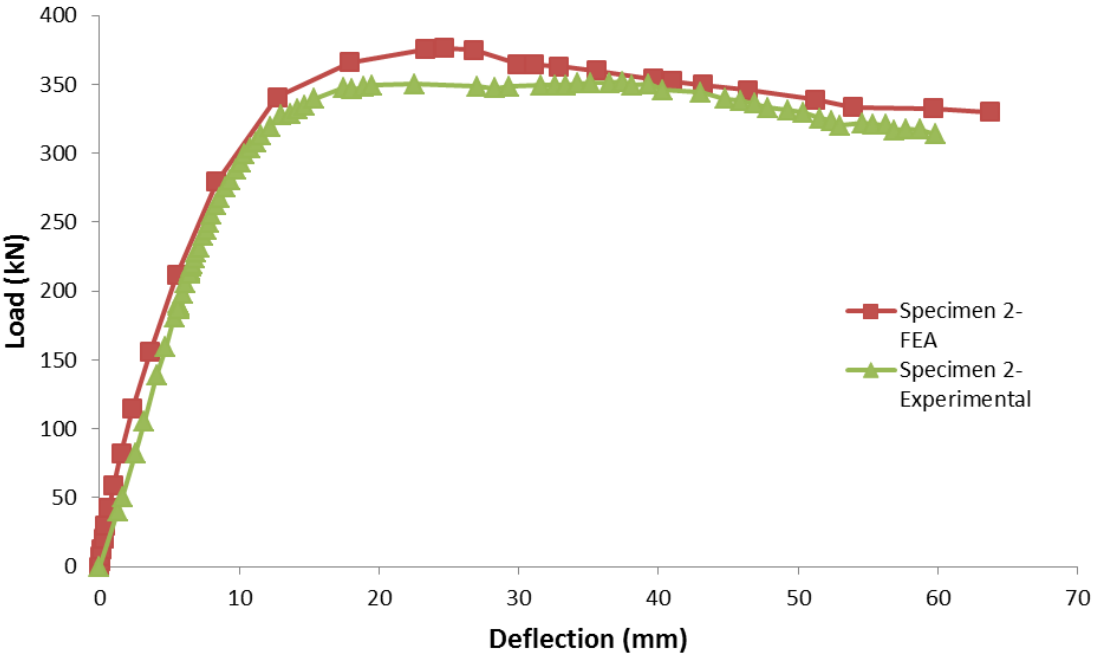

Figure 5.8: Comparison of load-displacement curves of Specimen 2 - experimental and simulated

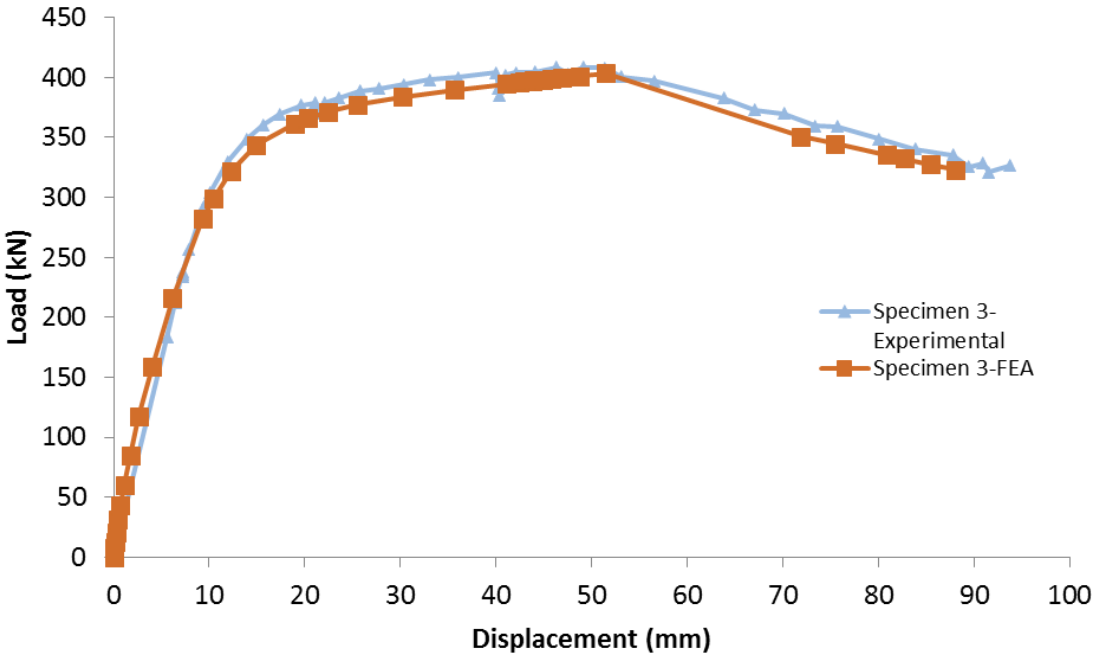

Figure 5.9: Comparison of load-displacement curves of Specimen 3 - experimental and simulated

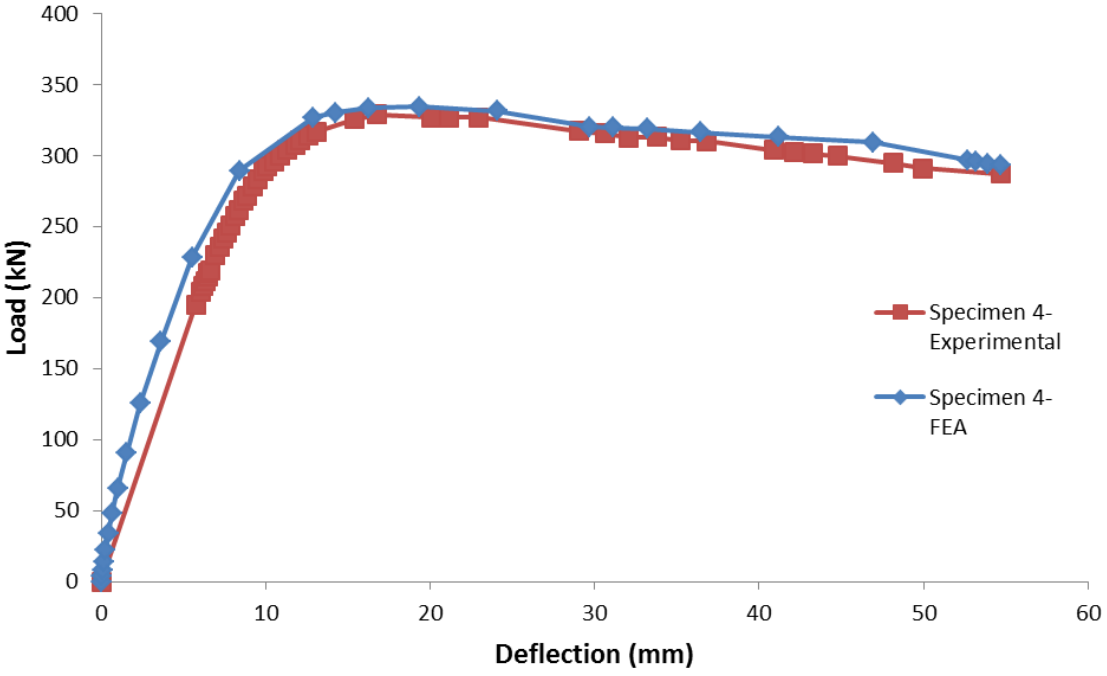

Figure 5.10: Comparison of load-displacement curves of Specimen 4 - experimental and simulated

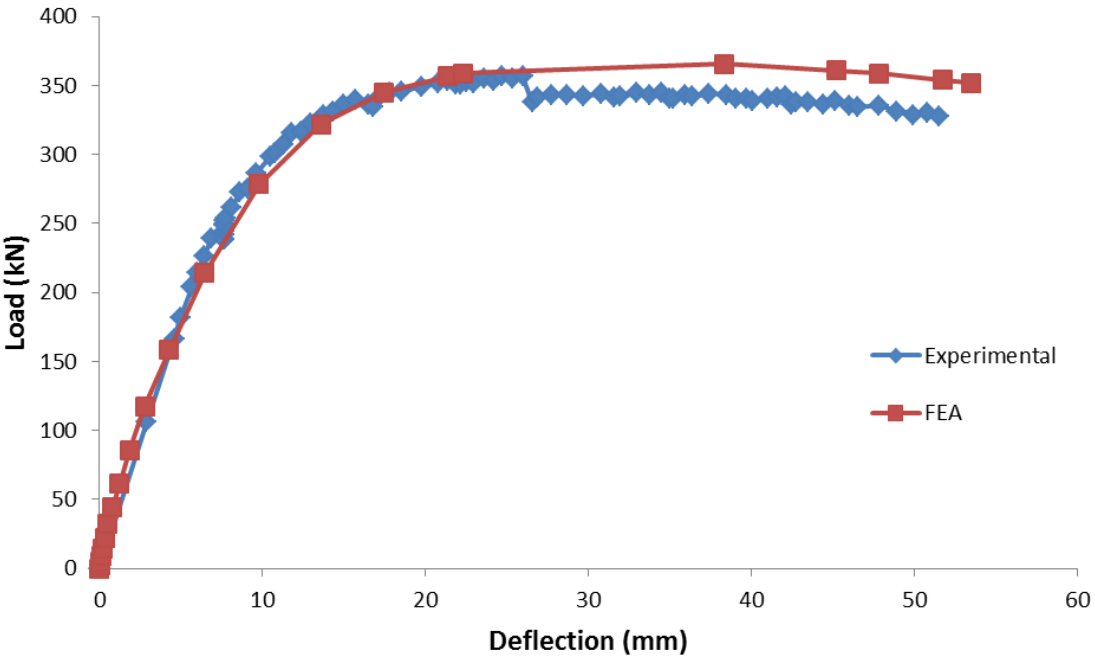

Figure 5.11: Comparison of load-displacement curves of Specimen 5 - experimental and simulated

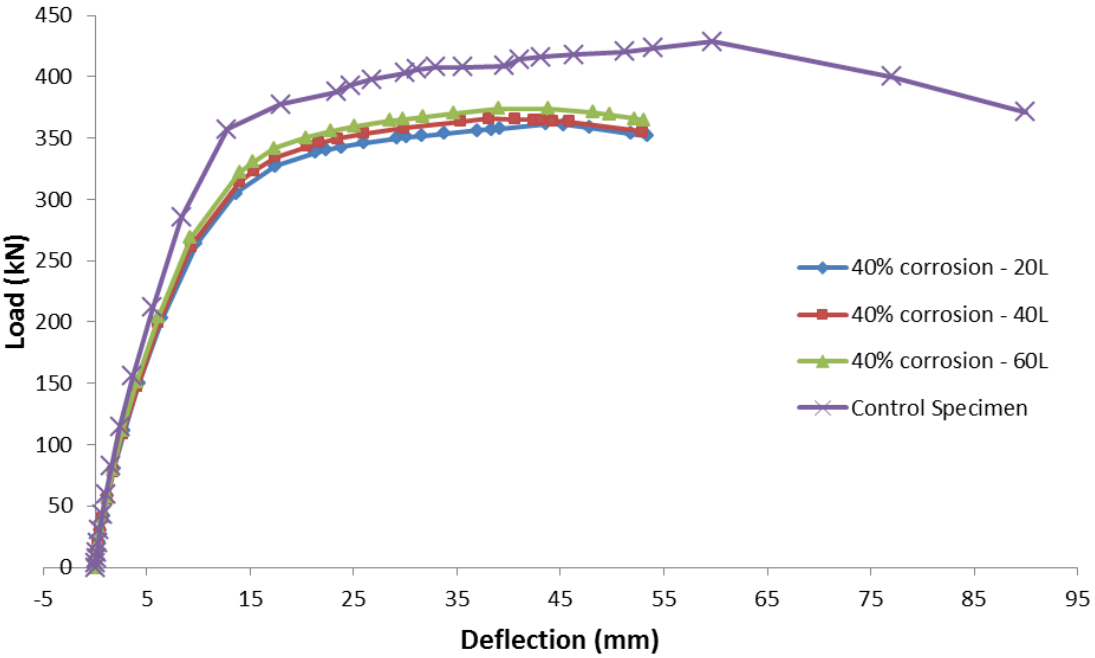

Figure 5.12: Comparison of load-displacement curves of Specimen 5 with varying number of layers of BFRP attached longitudinally

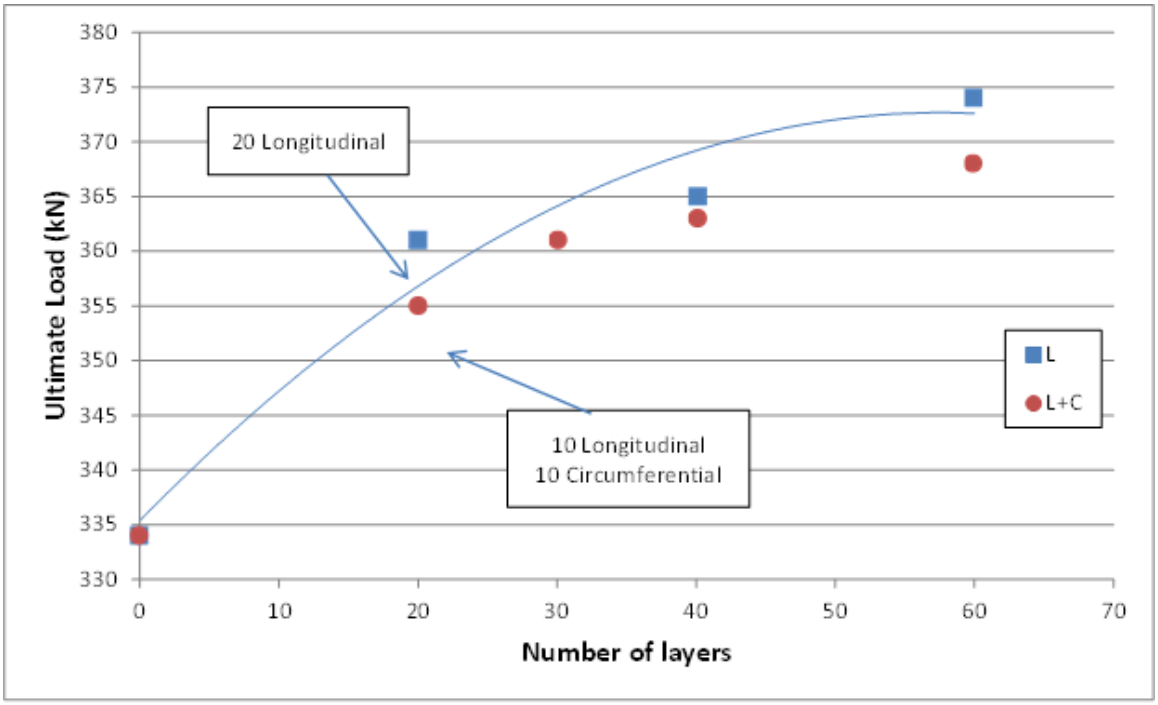

Figure 5.13: Comparison of amount of layers used for the repair of a pipe specimen with 40% corrosion

Chapter 6 Conclusions and Recommendations

The purpose of this project was to study the bending behaviour of pipes, and to analyze and document the effectiveness of basalt fabrics in repairing corroded pipes subjected to bending. To that end, five full-scale laboratory experiments and a study using finite element analysis software was conducted. After analyzing the results, the following conclusions and recommendations are made.

1. The yield load and ultimate load decrease as the corrosion depth increases.

2. Corrosion diminishes the effect of strain hardening and causes corroded pipes to reach their ultimate load capacity at a lower deflection.

3. As the corrosion depth of a pipe subjected to bending increases, the strain and the displacement needed for the initiation of a wrinkle decreases.

4. Addition of basalt FRP in the longitudinal direction delays the formation of a wrinkle and increases the displacement needed to reach the ultimate load.

5. Attaching BFRP composites with longitudinally angled fibres will improve the bending capacity of the pipe. However, as the number of layers increase, the ultimate load increases at a decreasing rate.

6. Fibres oriented in the circumferential direction, while necessary to carry the hoop stress of the pipe, do not increase the bending capacity of the pipe.

Since the basalt composite was only able to successfully repair the specimen with 1.2 mm of corrosion (20% of the wall thickness), it can be concluded that basalt fabric is only able to restore the bending capacity of pipes with a low amount of corrosion. A pre-cured

reinforcing sleeve may be able to restore the bending capacity of highly corroded pipes to that of an uncorroded pipe. Also, since attaching over twenty layers of fabric to one location of a pipe using the wet-layup system is impractical, a reinforcing sleeve made of basalt may be a better approach.

REFERENCES

AEA Technology Consulting. 2001. *Temporary/permanent Pipe Repair - Guidelines*. United Kingdom. http://www.hse.gov.uk/research/otopdf/2001/oto01038.pdf.

American Society of Mechanical Engineers. 1991. *ASME B31G: Manual for Determining the Remaining Strength of Corroded Pipelines*. https://law.resource.org/pub/us/cfr/ibr/002/asme.b31g.1991.pdf.

———. 2008. *ASME PCC-2 : Repair of Pressure Equipment and Piping*. *Asme*. Vol. 2008. https://www.asme.org/products/codes-standards/pcc2-2015-repair-pressure-equipment-piping-(1).

———. 2009. *ASME B31G: Manual for Determining the Remaining Strength of Corroded Pipelines*. http://marineman.ir/wp-content/uploads/2015/05/Manual-for-Determining-The-Remaining-Strength-of-Corroded-Pipelines.pdf.

ASTM C1161. 2017. *Standard Test Method for Flexural Strength of Advanced Ceramics at Ambient*. doi:10.1520/C1161-13.2.

ASTM D6272. 2017. "Standard Test Method for Flexural Properties of Unreinforced and Reinforced Plastics and Electrical Insulating Materials by Four-Point Bending 1." doi:10.1520/D6272-17.1.

Bai, Yong. 2001. *Pipelines and Risers*. Vol. 3. http://dlia.ir/Scientific/e_book/Technology/Hydraulic_Engineering/TC_1501_1800_Ocean_Engineering_/020678.pdf.

Chan, P., K. Tshai, M. Johnson, H. Choo, S. Li, and K. Zakaria. 2014. "Burst Strength of Carbon Fibre Reinforced Polyethylene Strip Pipeline Repair System - a Numerical and Experimental Approach." *Journal of Composite Materials* 49 (6): 749–56. doi:10.1177/0021998314525652.

Chen, Meiling. 2008. "Repair of Corroded Steel Beam Using CFRP Repair of Corroded Steel Beam Using CFRP."

Cosham, A, P Hopkins, and K A Macdonald. 2007. "Best Practice for the Assessment of Defects in Pipelines – Corrosion." *Engineering Failure Analysis* 14: 1245–65. doi:10.1016/j.engfailanal.2006.11.035.

Cosham, Andrew, and Phil Hopkins. 2004. "An Overview of the Pipeline Defect Assessment Manual (Pdam)" 44 (May): 1–13.

———. 2005. "THE PIPELINE DEFECT ASSESSMENT MANUAL (PDAM)." http://www.novinparsian.ir/CMS_UI/images/Download/The Pipeline Defect Assessment Manual (PDAM)-Cosham_opt.pdf.

Cuthill, Jim. 2002. “Advances In Materials, Methods, Help Gain New Users.”

Dewanbabee, Halima. 2009. “Behaviour of Corroded X46 Steel Pipe under Internal Pressure and Axial Load.” University of Windsor.

Dewanbabee, Halima, and Sreekanta Das. 2013. “1 . Structural Behavior of Corroded Steel Pipes Subject to Axial Compression and Internal Pressure : Experimental Study.” *Journal of Structural Engineering (United States)* 139: 57–65. doi:10.1061/(ASCE)ST.1943-541X.0000596.

Duell, J M, J M Wilson, and M R Kessler. 2008. “Analysis of a Carbon Composite Overwrap Pipeline Repair System.” *International Journal of Pressure Vessels and Piping* 85 (11). Elsevier Ltd: 782–88. doi:10.1016/j.ijpvp.2008.08.001.

Elchalakani, Mohamed. 2016. “Rehabilitation of Corroded Steel CHS under Combined Bending and Bearing Using CFRP.” *Journal of Constructional Steel Research*. Elsevier Ltd.

EWI. 2003. *Strain-Based Design of Pipelines*. http://documents.mx/documents/strain-based-design-ewi.html.

ISO/TS 24817. 2006. *Petroleum, Petrochemical and Natural Gas Industries — Composite Repairs for Pipework — Qualification and Design, Installation, Testing and Inspection*. Vol. 2006.

Ju, G T, and S Kyriakides. 1991. “Bifurication and Localization Instabilities In Cylindrical Shells Under Bending Part II Predictions.”

Lim, K S, S N A Azraai, N M Noor, and N Yahaya. 2015. “An Overview of Corroded Pipe Repair An Overview of Corroded Pipe Repair Techniques Using Composite Materials,” no. April 2016. http://waset.org/publications/10003226/an-overview-of-corroded-pipe-repair-techniques-using-composite-materials.

Limam, A, L Lee, E Corona, and S Kyriakides. 2010. “Inelastic Wrinkling and Collapse of Tubes under Combined Bending and Internal Pressure.” *International Journal of Mechanical Sciences* 52 (5). Elsevier: 637–47. doi:10.1016/j.ijmecsci.2009.06.008.

Meniconi, Luiz C M, José L.F. Freire, Ronaldo D. Vieira, Jorge L.C. Diniz. 2002. “STRESS ANALYSIS OF PIPELINES WITH COMPOSITE REPAIRS,” 1–7. http://pipingrepairtechnologies.com/wp-content/uploads/2009/04/petrobras-composite-stress-analysis.pdf.

NACE International. 2002. “Corrosion Costs and Preventive Strategies in the United States.”

Natural Gas STAR Partners. n.d. “Composite Wrap for Non-Leaking Pipeline Defects.” https://www.epa.gov/sites/production/files/2016-06/documents/ll_compwrap.pdf.

Nazemi, Navid. 2009. “Scholarship at UWindsor Behavior of X60 Line Pipe under Combined Axial and Transverse Loads with Internal Pressure.”

Prabhu, Shivananda. 2016a. “An Intro to Pipeline Corrosion and Coatings.pdf.” *Corrosionpedia*. https://www.corrosionpedia.com/2/1383/corrosion-101/an-intro-to-pipeline-corrosion.

———. 2016b. “Corrosion Prevention for Buried Pipelines.pdf.” *Corrosionpedia*. https://www.corrosionpedia.com/2/2652/corrosion-prevention/corrosion-prevention-for-buried-pipelines.

Shouman, Ahmed, and Farid Taheri. 2009. “An Investigation Into The Behaviour Of Composite Repaired Pipelines Under Combined Internal Pressure and Bending.” *Proceedings of the ASME 2009 28th International Conference on Ocean, Offshore and Arctic Engineering*.

Whai, Sam Cheok. 2014. “The Repair Option.” http://www.alstern-technologies.com/Articles/The Repair Option.pdf.

Yoosef-Ghodsi, Nader, J J Roger Cheng, and David W Murray. 2000. “IPC2000-213 Analytical Simulation and Field Measurements for a Wrinkle on the Norman.”

Yudo, Hartono, and Takao Yoshikawa. 2015. “Buckling Phenomenon for Straight and Curved Pipe under Pure Bending,” 94–103. doi:10.1007/s00773-014-0254-5.

VITA AUCTORIS

NAME:	Sachith Jayasuriya
PLACE OF BIRTH:	Kandy, Sri Lanka
YEAR OF BIRTH:	1993
EDUCATION:	*BASc – Civil Engineering, 2015* *University of Windsor*